Received: 28 January 2020 | Revised: 8 July 2020 | Accepted: 9 July 2020

DOI: 10.1111/psyp.13683

ORIGINAL ARTICLE

PSYCHOPHYSIOLOGY SPR WILEY

Neural measures of working memory in a bilateral change detection task

Tobias Feldmann-Wüstefeld

School of Psychology, University of Southampton, Southampton, UK

Correspondence
Tobias Feldmann-Wüstefeld, School of Psychology, University of Southampton, Highfield Campus B44, Southampton SO171BJ, UK.
Email: tobias.fw@soton.ac.uk

Abstract

The change detection task is a widely used paradigm to examine visual working memory processes. Participants memorize a set of items and then, try to detect changes in the set after a retention period. The negative slow wave (NSW) and contralateral delay activity (CDA) are event-related potentials in the EEG signal that are commonly used in change detection tasks to track working memory load, as both increase with the number of items maintained in working memory (set size). While the CDA was argued to more purely reflect the memory-specific neural activity than the NSW, it also requires a lateralized design and attention shifts prior to memoranda onset, imposing more restrictions on the task than the NSW. The present study proposes a novel change detection task in which both CDA and NSW can be measured at the same time. Memory items were presented bilaterally, but their distribution in the left and right hemifield varied, inducing a target imbalance or "net load." NSW increased with set size, whereas CDA increased with net load. In addition, a multivariate linear classifier was able to decode the set size and net load from the EEG signal. CDA, NSW, and decoding accuracy predicted an individual's working memory capacity. In line with the notion of a bilateral advantage in working memory, accuracy, and CDA data suggest that participants tended to encode items relatively balanced. In sum, this novel change detection task offers a basis to make use of converging neural measures of working memory in a comprehensive paradigm.

KEYWORDS

contralateral delay activity (CDA), electroencephalography (EEG), multivariate linear classifier, negative slow wave (NSW), working memory

1 | INTRODUCTION

Visual working memory describes the ability to maintain visual information over short periods of time. This is a crucial function of the visual system as it allows to retrieve and manipulate information not currently present to the senses. Studies of change blindness illustrated severe limitations of working memory processes (e.g., Simons & Levin, 1997) and inspired research that tried to pinpoint the properties of working memory. One fundamental property of working memory is its limited capacity (Baddeley, 2003; Luck & Vogel, 2013; Oberauer, Farrell, Jarrold, & Lewandowsky, 2016). Working

memory capacity is highly correlated with many cognitive functions such as fluid intelligence, attentional control, or school grades (Adam, Robison, & Vogel, 2018; Engle, Tuholski, Laughlin, & Conway, 1999; Krumm, Ziegler, & Buehner, 2008; Xu, Adam, Fang, & Vogel, 2018) which makes it a valuable tool to examine individual differences.

A well-established paradigm that measures working memory capacity is the *change detection task* (Luck & Vogel, 1997; Phillips, 1974; Zhang & Luck, 2008). In a change detection task, participants are first presented with a number of objects they have to encode into working memory. During a retention interval of typically 500–2,000 ms participants cannot see the objects anymore and need to maintain them in working memory. In a final test display, working memory is probed by presenting one (or more) of the items again. Participants indicate whether a change occurred or not. Change detection accuracy is precise for up to 3–4 items and then, drops drastically (Luck & Vogel, 1997). Taking guessing rate into account, an established way to estimate an individual's working memory capacity is using Cowan's K: K = N × (hit rate—false alarm rate) where K is the working memory capacity and N is the set size. In line with Luck and Vogel's (1997) findings, the estimated working memory capacity K is typically around 3–4 items (Cowan, 2001).

1.1 | The negative slow wave

The negative slow wave (NSW) was identified as a neural measure of working memory load, (Fukuda, Mance, & Vogel, 2015; Ruchkin, Johnson, Grafman, Canoune, & Ritter, 1992). The NSW was originally found by Ruchkin et al. (1992) in a change detection task with non-lateralized stimuli. Three, four, or five pairs of letters were presented to participants and then, shown again after 5 s with (change) or without (no change) a slight displacement of one of the pairs. The ERP elicited by the memory display was increasingly negative with an increasing set size. Because of its late onset (post P300) and sustained set size sensitivity (>3 s) this ERP component was described as a negative *slow* wave. This NSW set size effect was replicated with number of faces (Ruchkin, Johnson, Grafman, Canoune, & Ritter, 1997), number of color patches (Fukuda et al., 2015; Klaver, Smid, & Heinze, 1999), and number of occupied locations in a Sternberg delayed-match-to-sample task paradigm (Liu et al., 2018). The NSW is most pronounced at posterior electrode sites for spatial working memory tasks but also has a positive counterpart at more frontal sites in object working memory tasks (Mecklinger & Pfeifer, 1996). The NSW is correlated with working memory capacity K: the NSW amplitude is more pronounced for individuals with high working memory capacity (Liu et al., 2018; Wiegand et al., 2014) and asymptotes at working memory capacity (Fukuda et al., 2015). The NSW also seems to track dynamic changes in the memory load. One study used a change detection task with two targets and found that when a retro-cue reduced working memory load from two to one item, NSW amplitude was reduced compared to a neutral retro-cue that did not reduce working memory load (Schneider, Barth, Getzmann, & Wascher, 2017). This suggests that NSW amplitude may be sensitive to dropping of items from working memory, similar to the CDA (Kuo, Stokes, & Nobre, 2012). In sum, the NSW meets both the criterion for a neural correlate of current working memory load and working memory capacity limit. In contrast to the CDA, NSW can be elicited by centrally (Ruchkin et al., 1992) or bilaterally (Fukuda et al., 2015) presented stimuli, that is, it is not required to cue participants to either hemifield.

1.2 | The contralateral delay activity

An important innovation for working memory research was the discovery of a further ERP component that reflects working memory load, the *contralateral delay activity (CDA)*. The CDA was first described in a lateralized version of a change detection task (Vogel & Machizawa, 2004; Vogel, McCollough, & Machizawa, 2005). Instead of trying to remember all items presented in the memory display, participants only had to encode and maintain items from either the left or right hemifield, as only items from that side would be probed in the end of a trial. Prior to the onset of the memory display, a cue indicated which side would be relevant in the current trial. Vogel and Machizawa (2004) found a sustained contralateral negativity to cued items that lasted until the test display was shown (hence contralateral *delay* activity). Because the CDA is the difference between the contra- and ipsilateral signal, task-unspecific activity that affects both hemispheres is canceled out (Gratton, 1998). Thus it was argued that the CDA is a better measure of working memory load than the NSW (Drew, McCollough, & Vogel, 2006). The CDA has important properties that renders it a valuable tool in working memory research. The CDA amplitude increases with increasing set size, suggesting it reflects the current number of items held in working memory (Feldmann-Wüstefeld, Vogel, & Awh, 2018; Vogel & Machizawa, 2004). In line with this notion, the CDA did not linearly increase but asymptoted right around the point of an individual's working memory capacity (Balaban & Luria, 2015a; Unsworth, Fukuda, Awh, & Vogel, 2014; Vogel et al., 2005), suggesting that once working memory capacity is reached, CDA as a measure of items held in working memory cannot increase furthermore, similar to the NSW. Working memory capacity is closely linked to cognitive abilities such as reading skills, arithmetic calculation, and fluid intelligence (Baddeley, 2003; Unsworth, Brewer, & Spillers, 2009) and the CDA, as a measure of

working memory, has also been linked to track individual differences in cognitive abilities (Unsworth, Fukuda, Awh, & Vogel, 2015). In addition, the CDA amplitude is reduced in individuals with impaired working memory, for example, ADHD patients (Wiegand et al., 2016) or elderly adults (Wiegand, Finke, Müller, & Töllner, 2013). In the present study, a revised change detection paradigm will be used that does not require participants to shift attention to one hemisphere in order to measure working memory processes. This may be particularly helpful for studies with participants with impaired cognitive abilities as the cognitive demands are presumably lower.

1.3 | Measuring NSW and CDA in the same task

The primary goal of the current study was to develop a working memory paradigm in which both the NSW as a non-lateralized and the CDA as a lateralized measure can be used. While the CDA has the advantage that task-unspecific effects on the EEG signal (such noise or bottom-up processing differences between conditions) are canceled out through the contralateral control method (Gratton, 1998), the NSW has several advantages as well. For example, the CDA increase with set size may not only be due to more targets in the attended hemifield, but also due to more distractors in the opposite hemifield (Fukuda et al., 2015; Sauseng et al., 2009), whereas no distractor variations are required for NSW designs. Furthermore, the NSW has the advantage that it does not require a spatial cue to direct participants' attention to one hemifield. Cue-related activity can contaminate working memory-related EEG activity (Cooreman, Wiegand, Petersen, Vangkilde, & Bundesen, 2015; Wiegand et al., 2018) and cue properties themselves can affect the working memory consolidation; for example, the more selective a cue, the stronger are neural working memory representations (Herrero, Nikolaev, Raffone, & van Leeuwen, 2009). Directing attention to the wrong hemifield may result in failures to encode items into working memory (but see Adam et al., 2018). Furthermore, cue-induced attention processes can complicate the interpretation of what is assumed a working memory modulation. For example, an apparent working memory effect may be due to one experimental condition benefitting more from an attention shift prior to memoranda presentation than another. Moreover, recognizing a cue, interpreting its meaning and then, directing attention according to the cue on the one hand, and encoding items into working memory on the other hand, may constitute a dual-task situation that increases task load, particularly when the relevant hemifield switches from trial to trial (Sander, Werkle-Bergner, & Lindenberger, 2011). Avoiding additional attentional demands can be helpful when comparing groups that could be differentially affected by them, for example, young and older adults or psychiatric patients and a control group. The paradigm used here will forgo cues and use the relative distribution of targets in the left and right hemifield to induce a lateralized signal.

1.4 | Hemisphere-specific contralateral activity

As pointed out above, one benefit of the CDA is that the subtraction of ipsi- from contralateral activity cleans the waveform from low level and early perceptual processing and leaves working memory-related activity (Gratton, 1998; Luria, Balaban, Awh, & Vogel, 2016). However, this comes with the drawback that any variation in the CDA amplitude could reflect a change in the contralateral activity, the ipsilateral activity, or both. The specific response of contra- and ipsilateral activity could go unnoticed which is why some studies focused on contra- or ipsilateral activity separately (Arend & Zimmer, 2011; Liesefeld, Liesefeld, & Zimmer, 2014). For example, Arend and Zimmermann (2011) used a change detection task in which a cue indicated from which side items were to be memorized. The number of targets (cued side) and distractors (uncued side) was systematically varied. For high memory loads (two or three targets), contralateral activity reflected the number of targets, irrespective of the number of distractors, and ipsilateral activity was neither affected by the number of targets nor the number of distractors. For low memory loads (one target), both contralateral and ipsilateral activity increased with distractor load. These results suggest that for a sufficiently high memory load, completely lateralized processing takes place that is determined by the number of items in the relevant hemifield (targets) but unaffected by the number of items in the irrelevant hemifield (distractors). For low memory loads, however, distractors get processed to some extent (Arend & Zimmer, 2011), possibly because leftover working memory capacity is automatically used for distractors (Lavie, 2005). In the present study, there will be targets in *both* hemifields which will allow to compare the activity contralateral to one subset of targets (e.g., the high-load hemifield) with the activity contralateral to another subset of targets (e.g., the low-load hemifield). To address the question of how targets compete for access to working memory, one question will be how the contralateral activity to four targets varies as a function of whether 0 or 2 targets are presented in the ipsilateral hemifield. Results will be informative regarding the notion that target processing is mainly reflected in the EEG signal contralateral to the target (Arend & Zimmer, 2011; Liesefeld et al., 2014) and in how far processing of targets

in one hemisphere is affected by the number of targets in the opposite hemifield.

1.5 | Information-based decoding approach

Besides event-related potentials, an information-based decoding approach (Bae & Luck, 2018, 2019) will be used that measures the information content present in the neural signals of each individual participant to quantify working memory processes. Information-based decoding methods are multivariate approaches originally popularized by brain-computer interfaces (Bigdely-Shamlo, Vankov, Ramirez, & Makeig, 2008; Thulasidas, Guan, & Jiankang, 2006) but now becoming increasingly popular in cognitive neuroscience as a tool to assess how much information is present in a given neural signal (Bae, Leonard, Hahn, Gold, & Luck, 2020). This means that instead of asking how an experimental manipulation affects the neural signal (e.g., a voxel or EEG electrode), the question is: How much information about the experimental manipulation is present in the neural signal? For example, the *orientation* of an item in working memory can be decoded from fMRI data (Ester, Sprague, & Serences, 2015) or the unfiltered EEG signal (Bae & Luck, 2018) and the *location* of an item in working memory can be decoded from alpha-band activity in the EEG data (Foster, Sutterer, Serences, Vogel, & Awh, 2016). The basic principle of information-based decoding approaches is to train a classifier in a subset of trials so that it differentiates between conditions of interest as well as possible. In a second step, the classifier is tested in an independent set of trials in terms of how accurately it can classify the trials as the respective condition. Multivariate classifiers have recently been shown to allow decoding working memory content (Bae & Luck, 2018; Foster et al., 2016), but these studies have decoded target identity or location, whereas the current study will aim to decode the number of targets (set size) or the target imbalance (net load). In the present study, the classifier will be trained and tested time-point by time-point to allow tracking how much information is contained in the EEG signal about set size/net load in a time-resolved manner. Such a classifier may prove as a valuable tool to track working memory processes as multivariate approaches can pick up on variations in the neural data that go unnoticed with the relatively coarse method of ERPs. Furthermore, multivariate tracking of working memory load is generalizable across stimuli, tasks, observers, and experiments and thus a particularly flexible tool (Adam, Vogel, & Awh, 2020).

1.6 | Rationale of the present study

The present study uses a novel, bilateral change detection paradigm that can provide a framework of converging neural markers of working memory. The paradigm presents a variable number of targets bilaterally, similar to traditional NSW tasks (Fukuda et al., 2015; Schneider et al., 2017), however with targets being unequally distributed in both hemifields. Although a CDA is typically observed contralateral to a cued hemifield, previous studies also showed that a CDA can result from target imbalances, for example, when targets are only presented in one hemifield (Feldmann-Wüstefeld & Vogel, 2018), from successive presentation of targets in the left and right hemifield (Berggren & Eimer, 2016; Feldmann-Wüstefeld et al., 2018), or when a single target is presented in one hemifield of a visual search task (Feldmann-Wüstefeld, Busch, & Schubö, 2019; Jolicœur, Brisson, & Robitaille, 2008; Töllner, Conci, Rusch, & Müller, 2013). Thus, in the present study, instead of using a cue that directs attention toward one hemifield, the spatial imbalance is inherent of the target distribution itself. For example, three targets may be presented in the left hemifield and one target in the right hemifield. This constitutes a net load of two items in the left hemifield which should accordingly elicit a CDA contralateral to the left hemifield. The target imbalance, however, is only a "cognitive" imbalance. To keep physical stimulation balanced between hemifields, both hemifields will be filled up with distractors, that is, irrelevant items that will not be probed in the end of a trial and can thus be safely ignored. For example, when three targets are presented in the left hemifield and one target in the right hemifield, three distractors will be presented in the left hemifield and five distractors in the right hemifield. As a result, the total number of items in both hemispheres is equal and fixed across conditions.

This study has six goals. First, it will be measured whether the non-lateralized NSW is sensitive to working memory load. Previous studies showed that the NSW increases with number of bilateral targets but in the present study, the total number of items (targets + distractors) will be kept constant which will allow to unlink the NSW from total stimulation.

Second, it will be measured whether the unequal distribution of targets induces a processing imbalance (net load) measurable as a contralateral negativity (CDA) to the hemifield with more targets. Attention needs to be deployed toward both hemifields, but a different number of targets needs to be encoded from each hemifield (net load). The CDA amplitude is expected to increase with net load.

Third, it will be measured whether the activity in a given hemisphere is determined by the number of targets in the contralateral hemifield. The negativity contralateral to a fixed number of targets may vary as a function of the number of targets in the other hemifield, thus revealing competition for access to working memory.

Fourth, variations within net load and accuracy may reveal how targets are sampled. Targets could be entirely randomly selected or participants might have a preference to encode them from the more numerous (high-load) hemifield

or the less numerous (low-load) hemifield. A model based on behavioral performance and CDA amplitude will be used that estimates how likely a target enters working memory as a function of the hemifield in which it is presented.

Fifth, a multivariate linear classifier will be trained to assess whether it can decode set size and net load, similar to previous studies that showed working memory features and location can be decoded from the EEG signal.

Sixth, NSW, CDA, and decoding accuracy will be tested as predictors of working memory capacity K to examine whether these neural measures are functionally significant.

2 | METHOD

2.1 | Participants

Twenty-one volunteers, naïve to the objective of the experiment participated for payment. Participants were aged 18–31 years ($M = 22.8$, $SD = 4.3$), 10 of them were male, 20 of them were right-handed, and all of them reported normal or corrected-to-normal visual acuity. Normal color vision was assured with an Ishihara color test. As no participant had more than 25% of artifact-contaminated trials (see below for criteria), the entire sample was used for analysis. The experiment was conducted with the written understanding and consent of each participant. Experimental procedures were approved by the local ethics committee.

2.2 | Apparatus

Participants were seated in a comfortable chair in a dimly lit, electrically shielded, and sound attenuated chamber. Participants responded with button presses on a standard U.S. American QUERTY keyboard that was placed in front of them. Stimulus presentation and response collection were controlled by a Windows PC. Experiments were written in MatLab with the Psychophysics Toolbox extensions (Kleiner et al., 2007). All stimuli were presented on a LCD-TN screen (BenQ XL2430-B) placed at ~75 cm distance from participants.

2.3 | Design

The experiment comprised a total of 1,560 trials run in 30 blocks of 52 trials. There were three different set sizes: participants had to remember two, four, or six targets. Crucially, within each set size condition, the "net load," that is, the imbalance between the left and right visual field, varied. In the following, the target distribution resulting in the different net loads will be denoted irrespective of left/right hemifield, for example, 2-1 refers to two targets in the left and one in the right hemifield or vice versa. There were eight conditions in total. For set size 2, there were two conditions: a net load 2 condition with two targets in one hemifield and none in the other (2-0; 240 trials) and a net load 0 condition with a target in both hemifields (1-1; 120 trials). For set size 4, net load conditions was 0 (2-2; 120 trials), 2 (3-1; 240 trials), or 4 (4-0; 240 trials). Analogously, for set size 6, three net load conditions of 0 (3-3; 120 trials), 2 (4-2; 240 trials), and 4 (5-1; 240 trials) were used. For each of the five lateralized conditions (with net load 2 or 4), the left and the right hemifield showed the more numerous subset of targets equally likely.

2.4 | Stimuli

All stimuli were presented on a gray background (RGB: 128-128-128). The fixation cross was black (0-0-0) and had a diameter of 0.5° visual angle. Targets were colored circles with a diameter of 1.5° (see Figure 1). Distractors were colored squares with a side length of 1.33° (i.e., of equal area as circles). Memory displays always showed 12 items, that is, two targets and 10 distractors, four targets and eight distractors or six targets and six distractors. All 12 items were distributed on a 6×6 grid. In each quarter, there were three items and targets were as equally distributed across quarters as possible. The distance between the center of grids was 2.2°, or 4° for grid cells left and right of the vertical midline. Thus the overall diameter of the grid was $12.8° \times 11.0°$. Within the grid, items were jittered by -2, -1, 0, 1, or $2 \times 0.15°$. Colors for squares and circles were drawn randomly from a set of 13 colors (red [255-0-0], light green [0-255-0], blue [0-0-255], yellow [255-255-0], magenta [255-0-255], cyan [0-255-255], dark green [30-140-60], purple [128-0-255], orange [255-128-0], brown [157-0-23], rosé [255-174-201], black [0-0-0] or white [255-255-255]). No color was repeated within one memory display. The probe display showed a circle at one of the target positions (randomly chosen). It had the same color as the target from the memory display in 50% of the trials (no change trials) and the color not used in the memory display in the remaining 50% of the trials (change trials).

2.5 | Procedure

Prior to each trial, a "ready" display was presented that only showed a central black fixation dot (0.5°). The ready display indicated for the participant to fixate the center and prepare for the upcoming trial. After participants pressed spacebar to begin, the trial started with a fixation cross that was presented for 500 ms (see Figure 1). The memory display followed and was presented together with a fixation cross for 500 ms. Participants were instructed to remember the color

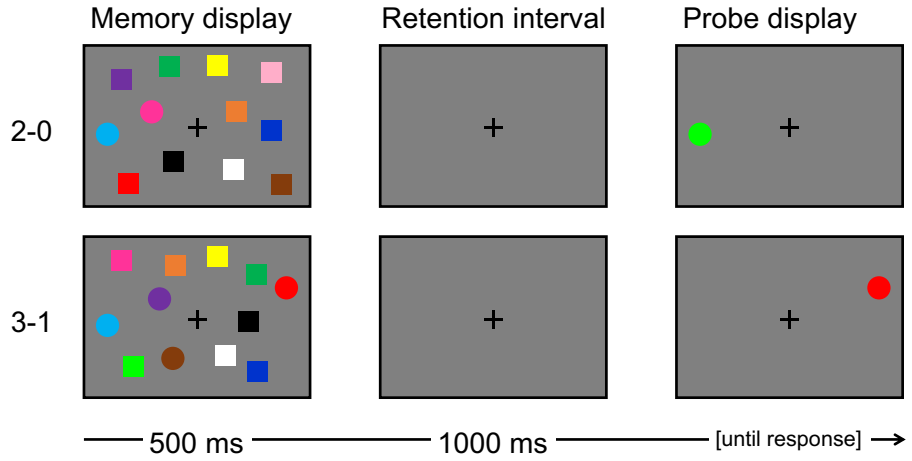

FIGURE 1 Stimuli and trial procedure. Participants were asked to memorize circles and ignore squares in the memory display. The upper row shows an example with a target distribution of 2-0, the lower row with a target distribution of 3-1 (further target distributions not shown here: 1-1, 2-2, 3-3, 4-0, 4-2, and 5-1). For each target distribution, the left and right hemifield were equally likely the high-load hemifield (i.e., 3-1 and 1-3 were equiprobable). The total number of items was always 12. The probe display showed one of the circles at the same location as in the memory display and participants were asked to indicate whether the circle had the same (no change trials, lower row example) or a different color (change trials, upper row example).

and location of the circles and ignore all squares. All eight memory conditions were randomly shuffled across the experiment. The memory display was followed by a retention interval of 1,000 ms in which only a fixation cross was shown. The probe display followed and was presented until participants pressed one of the two response buttons. Participants were instructed to press the left button ("z") with their left index finger for "same color" (circle at probed location did not change color compared to the memory display) and to press the right button ("?") with their right index finger for "different color" (circle at probed location did change color). They were instructed to respond as accurately as possible. The trial ended with the button press and a blank screen was presented during an 1,000 ms inter-trial interval before the next "ready" screen appeared. Performance feedback (average accuracy) and a minimum break of 10 s (participants decided when to continue) were provided after each block.

Gaze position was tracked at a sampling rate of 1,000 Hz for both eyes with an EyeLink 1,000 + eye tracker (SR Research Ltd., Mississauga, Ontario, Canada). A direct gaze feedback violation procedure was applied from 250 ms after fixation cross onset until the onset of the probe display, that is, for 1,750 ms. If participants' gaze was not within 1.5° of the center of the fixation cross during that time, or if they blinked, the trial was aborted, and a message "eye movement" (or, "blink") was presented on the screen before a ready screen indicated the restart of the next trial. The remaining trials were shuffled so as to put the aborted trial in a random position within the sequence and make its reappearance unpredictable. Accordingly, any detected gaze violation extended the experiment by one trial. The number of trials per block without gaze violation was kept constant at 52.

2.6 | EEG recording

EEG was recorded with Ag–AgCl "actichamp" active electrodes (BrainProducts, Gilching, Germany) from 32 scalp sites (according to the International 10/20 System: FP1/2, F7/8, F3/4, Fz, FC5/6, FC1/2, C3/4, Cz, TP9/10, CP5/6, CP1/2, P7/8, P3/4, PO7/8, PO3/4, Pz, O1/2, and Oz). Horizontal and vertical EOGs were recorded with passive electrodes bipolarly from the outer canthi of the eyes and from above and below the observers' right eye, respectively. FPz served as the ground electrode and all electrodes were referenced to TP10 and re-referenced off-line to the average of all electrodes. Impedances for active electrodes were kept below 10 kΩ. Sampling rate was 1,000 Hz with a high cutoff filter of 125 Hz and a low cutoff filter of 0.01 Hz (half power cutoff, 24 dB rolloff).

2.7 | Data analysis

All raw data and analysis scripts are available on Open Science Framework (https://osf.io/krv4p/).

2.7.1 | Behavioral data

Accuracy was calculated for each set size and forwarded to a 1 × 3 ANOVA for repeated measures. Within each set size, accuracy was compared between all target distributions with *t* tests for dependent measures. To reveal differences in how well items could be encoded from each hemifield, for the conditions 3-1, 4-2, and 5-1, accuracy

was compared for probing the high-load versus low-load hemifield with *t* tests for dependent measures (this analysis was not possible for the other conditions because they had symmetric displays or only targets in one hemifield). To calculate the working memory capacity measure K, hit rate (ratio of correctly identified changes) and correct rejection rate (ratio of correctly identified color repetitions) were determined separately for each set size, and across set size. K was calculated with Cowan's (2001) formula: K = N × (hit rate—false alarm rate).

2.7.2 | EEG data: Event-related potentials

Trials with eye-related artifacts from −200 to 1,500 ms were excluded from the analysis ($M = 7.7\%$, $SD = 5.5\%$). Eye-related artifacts were identified as eye tracking data indicating a gaze drift (>1° degrees from fixation) or saccades (difference in gaze position between first and second half of 50-ms time window >0.5°; time window moving in 20-ms steps). Additionally, segments were excluded from further analysis on an individual-channel basis when the absolute voltage exceeded 60 μV. Only correct trials were analyzed.

The NSW amplitude was most negative at PO7 and PO8 across conditions (see Figure 3). Thus for NSW analyses, mean activity for the electrode pool PO7/PO8 (bilateral) was calculated for Set Size 2, 4, and 6, and for net load 0, 2, and 4, resulting in six waveforms for each participant. The NSW amplitude was determined for a time windows of 500–1,500 ms and forwarded to a 1 × 3 ANOVA with the within-subjects factor Set Size and to a 1 × 3 ANOVA with the within-subjects factor net load. Amplitude of the CDA was most negative at PO7 and PO8 across time windows and conditions (see Figure 4). Thus for CDA analyses, the mean contralateral and ipsilateral (relative to high-load hemifield) ERP signal for the electrode pool PO7/PO8 was calculated for the five conditions with a net load >0 (2-0, 3-1, 4-0, 4-2, and 5-1). This resulted in 10 waveforms for each participant. The CDA was determined as the mean lateralized amplitude (difference contra minus ipsi to high-load hemifield) for a time window of 500–1,500 ms. The CDA was analyzed with a 2 × 2 ANOVA with the within-subjects factors laterality and net load (2, 4). CDA was further analyzed with a 2 × 5 ANOVA with the within-subjects factors Laterality (contra- vs. ipsilateral activity) and Target Distribution (2-0, 3-1, 4-0, 4-2, and 5-1). Planned comparisons within each net load compared the CDA for all possible target distributions. As contra- and ipsilateral activity responded differently to experimental manipulations, follow-up analyses compared conditions separately for contra- and ipsilateral sites (see results for details). Using the CDA data, a model estimated the encoding bias, that is, how likely participants encoded an items from the high-load versus low-load hemifield (see results for details).

2.7.3 | EEG data: Classifier

A multivariate linear classifier was used to assess whether set size or net load could be decoded from raw (unfiltered) EEG data that was previously shown to track attention deployment (Fahrenfort, Grubert, Olivers, & Eimer, 2016; see Foster et al., 2016 for decoding from alpha-band filtered EEG data). To that end an equal number of artifact-free trials was first selected from each set size or net load condition (e.g., if there were n artifact-free trials for set size 2, n + x for set size 4, and n + y for set size 6, n trials were randomly picked for each set size). Within each condition, the EEG signal was averaged across bins of 10 randomly selected trials and bins of five subsequent data points (i.e., 5 ms) to obtain a better signal-to-noise ratio. A total of 2/3 of available trial bins were assigned to a training set, the remaining 1/3 were assigned to a testing set. As opposed to ERP analyses, a trial was excluded from analysis if any electrode showed noise in that trial. Prior to this electrode-based rejection, all electrodes showing noise in more than 100 trials were excluded from the analysis to reduce the loss of trials. All remaining electrodes were treated equally and the model was blind to site, hemisphere etc. Using the Matlab function "classify.m," the classifier was tested in terms of how correctly it can classify set size or net load correctly in a given trial. Classification accuracy was calculated for each time bin of 5 ms from −200 to 1,500 ms. For cross-validation, the process of selecting trials and assigning them to trial bins as well as assigning them to training and testing bins, was repeated 100 times for each participant. Classification accuracy was averaged across the 100 iterations. As a control, the entire classification procedure described above was also applied to bins with shuffled labels (i.e., each trial was randomly assigned a net load or set size rather than using the correct label). The mean classification accuracy for the real data and the shuffled data were exported for the same time window as CDA and NSW (500–1,500 ms) and compared with a *t* test for dependent measures (one-tailed, as classification accuracy for shuffled data were expected to be worse than for real data). In addition, as an explorative measure, the same test was run for each time bin, to track the time course of classification accuracy. As a measure of effect size, partial eta squared (η^2) is reported for ANOVAs, Cohen's d for *t* tests. *T* test were one-tailed unless denoted otherwise. Greenhouse–Geisser correction was applied in all analyses when appropriate.

2.7.4 | Correlations

To assess how well neural measures of working memory predict an individual's working memory capacity, correlation analyses were run for working memory capacity measure

K (from trials with set sizes ≥ 4 as lower set sizes would underestimate K) on the one hand and mean NSW (across set sizes), mean CDA (across net loads), NSW increase ((SS4 + SS6)/2—SS2), CDA increase (NL4—NL2), and classification accuracy for set size and net load, on the other hand. Because not all variables were normally distributed, Spearman's rho (rank correlation coefficient) was used as a correlational measure.

3 | RESULTS

3.1 | Behavioral results (see Figure 2)

Accuracy varied as a function of set size (M_2 = 93.4%, M_4 = 82.5%, and M_6 = 74.7%), $F(2,40) = 238.3$, $p < .001$, and $\eta^2 = .92$. Accuracy for set size 2 was higher than for set size 4, $t(20) = 15.3$, $p < .001$, and $d = 3.33$, and set size 6, $t(20) = 16.8$, $p < .001$, and $d = 3.67$. Accuracy for set size 4 was higher than for set size 6, $t(20) = 11.3$, $p < .001$, and $d = 2.46$. Within each set size (2, 4, or 6), target distribution did not affect accuracy (all $t(20) \leq 1.7$, all $p \geq .057$, and all $d \leq 0.20$), except that 3-1 yielded a higher accuracy ($M = 83.2\%$) than 4-0 ($M = 81.4\%$), $t(20) = 2.3$, $p = .015$, and $d = 0.51$. For target distribution 3-1, accuracy was higher in trials in which the low-load hemifield ($M = 85.8\%$) compared to the high-load hemifield ($M = 82.2\%$) was probed, $t(20) = 3.0$, $p = .003$, and $d = 0.66$. Similarly, for target distribution 4-2, accuracy was higher in trials in which the low-load hemifield ($M = 77.4\%$) compared to the high-load hemifield ($M = 73.1\%$) was probed, $t(20) = 4.5$, $p < .001$, and $d = 0.98$. Again, for target distribution 5-1, accuracy was higher in trials in which the low-load hemifield ($M = 80.0\%$) compared to the high-load hemifield ($M = 74.2\%$) was probed, $t(20) = 2.9$, $p = .005$, and $d = 0.63$. The average advantage of the low-load hemifield (accuracy low-load/ accuracy high-load) was 5.8%. Overall working memory capacity K was 2.5 ($SD = 0.5$).

3.2 | Negative slow wave (bilateral ERP, see Figure 3)

NSW increased as a function of Set Size ($M_2 = -2.07$ μV, $M_4 = -2.37$ μV, and $M_6 = -2.42$ μV), $F(2,40) = 5.6$, $p = .013$, and $\eta^2 = .22$, see Figure 2a. Follow-up t tests for dependent measures showed that the ERP was different between SS2 and SS4 ($t(20) = 2.2$, $p = .021$, and $d = 0.48$), between SS2 and SS6 ($t(20) = 3.0$, $p = .004$, and $d = 0.65$), but not between SS4 and SS6 ($t(20) = 0.7$, $p = .240$, $d = 0.16$). NSW varied as a function of net load ($M_0 = -2.52$ μV, $M_2 = -2.21$ μV, and M4 = −2.23 μV), $F(2,40) = 6.6$, $p = .003$, and $\eta^2 = .25$. Follow-up t tests for dependent measures showed that the ERP was different between NL0 and NL2 ($t(20) = 4.5$, $p < .001$, and $d = 0.99$), between NL0 and NL 4 ($t(20) = 2.6$, $p = .009$, and $d = 0.56$), but not between NL2 and NL4 ($t(20) = 0.2$, $p = .411$, and $d = 0.05$). Only the 4-0 (but not the 5-1) condition was used for NL4 to achieve the same average set size across net load conditions. However, when including the 5-1 condition ($M_4 = -2.31$ μV), all statistical values were equivalent to using the 4-0 condition only.

3.3 | CDA (lateralized ERP, see Figure 4)

Note that the net load 0 conditions were not analyzed for the CDA as contra- and ipsilateral are not defined in these conditions. An interaction of laterality (contra, ipsi) and net load (2, 4) revealed that the CDA was larger for a net load of 4 (ΔM = 1.26 μV) than for a net load of 2 (ΔM = 0.78 μV), $F(1,20) = 13.8$, $p = .001$, and $\eta^2 = .41$. An interaction of Laterality (contra, ipsi) and Target Distribution (2-0, 3-1, 4-2, 4-0, and 5-1) revealed that the CDA amplitude varied as a function of relative distribution of targets in the visual field, $F(4,80) = 11.9$, $p < .001$, and $\eta^2 = .37$. The CDA was reliable in all five conditions (all $p \leq .001$). Within the net load 2 condition, the CDA was larger for a distribution

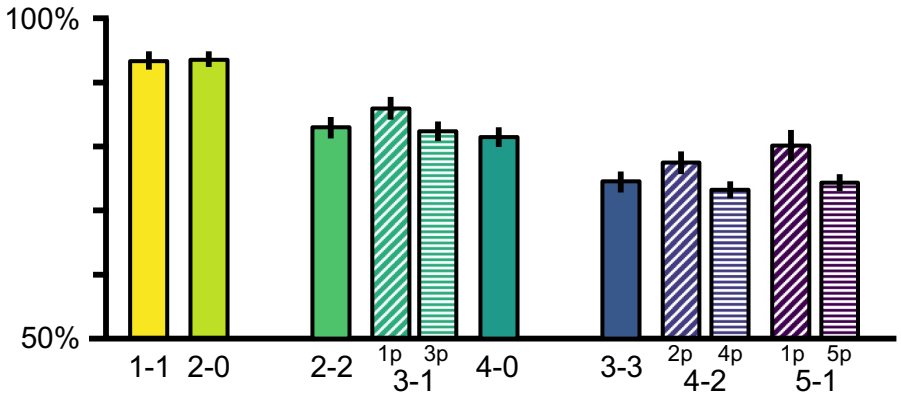

FIGURE 2 Mean accuracy for set size 2 (yellow shades), set size 4 (teal shades), and set size 6 (blue shades). For 3-1, 4-2, and 5-1, accuracy is shown separately for trials in which the low-load hemifield was probed (upward line pattern fill) and trials in which the high-load hemifield was probed (horizontal line pattern fill). Error bars denote standard error of the mean.

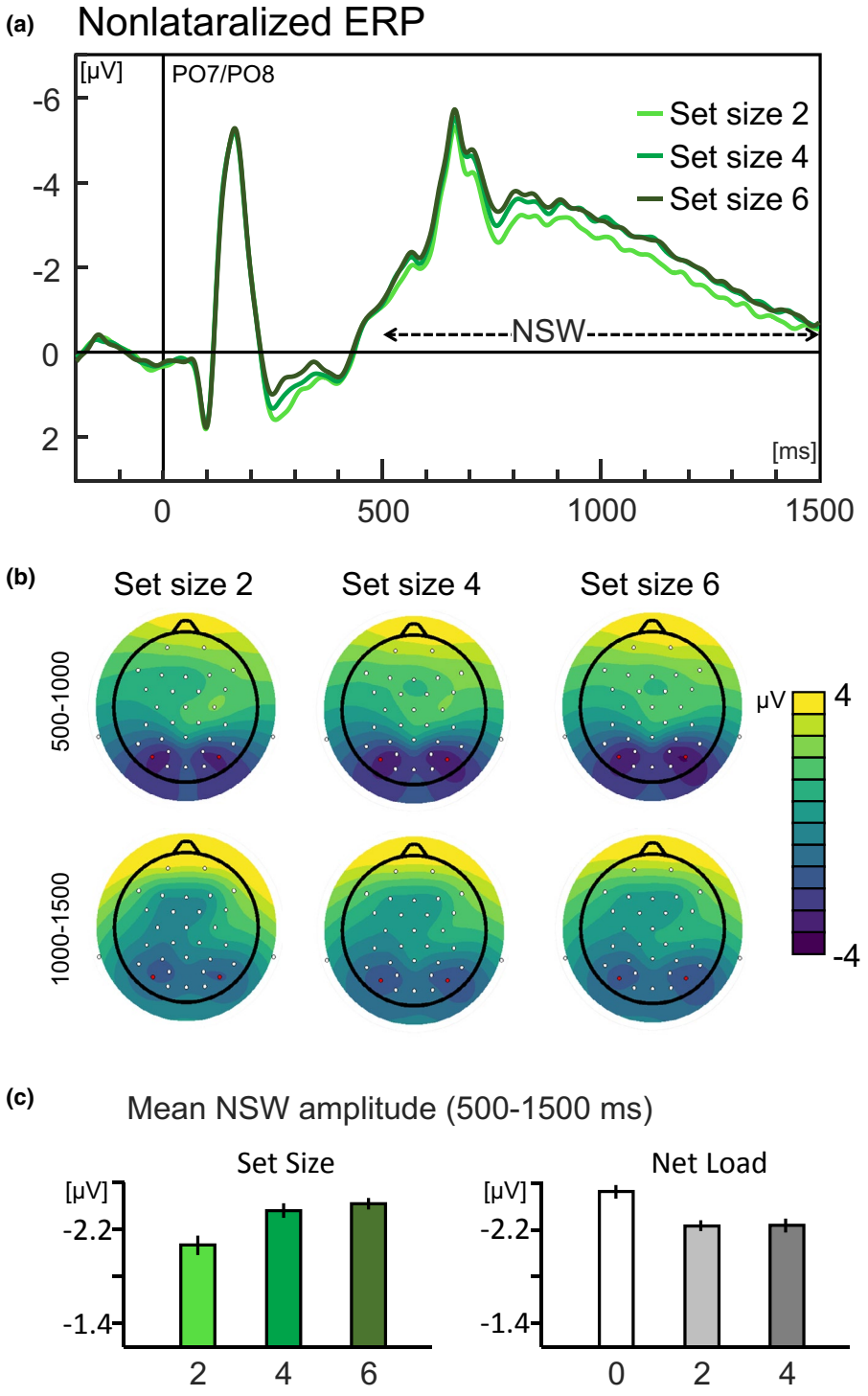

FIGURE 3 (a) Grand average bilateral waveforms, averaged across PO7/PO8, separately for Set Size 2, 4 and 6. For statistical analyses of the negative slow wave, the unfiltered average amplitude from 500–1,500 ms was used. For illustration purposes, waveforms shown here were low-pass filtered (non-causal Butterworth low-pass filter, half-amplitude cutoff = 30 Hz, slope = 24 dB/octave). (b) Topography of the average activity at each electrode site from 500–1,000 ms (upper row) and from 1,000–1,500 ms (lower row). (c) Average NSW amplitude from 500–1,500 ms, separately for set sizes (same data as in (A), left panel) and separately for net load 0, 2, and 4, right panel. Error bars denote standard errors of the mean, corrected for within-subjects comparisons (Cousineau, 2005)

of 2-0 ($\Delta M = -1.26$ μV) than for 3-1 ($\Delta M = -0.59$ μV), $t(20) = 3.8$, $p < .001$, and $d = 0.84$, and larger than for 4-2 ($\Delta M = -0.50$ μV), $t(20) = 4.4$, $p < .001$, and $d = 0.96$. The CDA was equally large for 3-1 and 4-2, $t(20) = 0.4$, $p = .335$, and $d = 0.09$. Within the net load 4 condition, the CDA was larger for a target distribution of 4-0 ($\Delta M = -1.49$ μV) than 5-1 ($\Delta M = -1.03$ μV), $t(20) = 3.9$, $p < .001$, and $d = 0.84$.

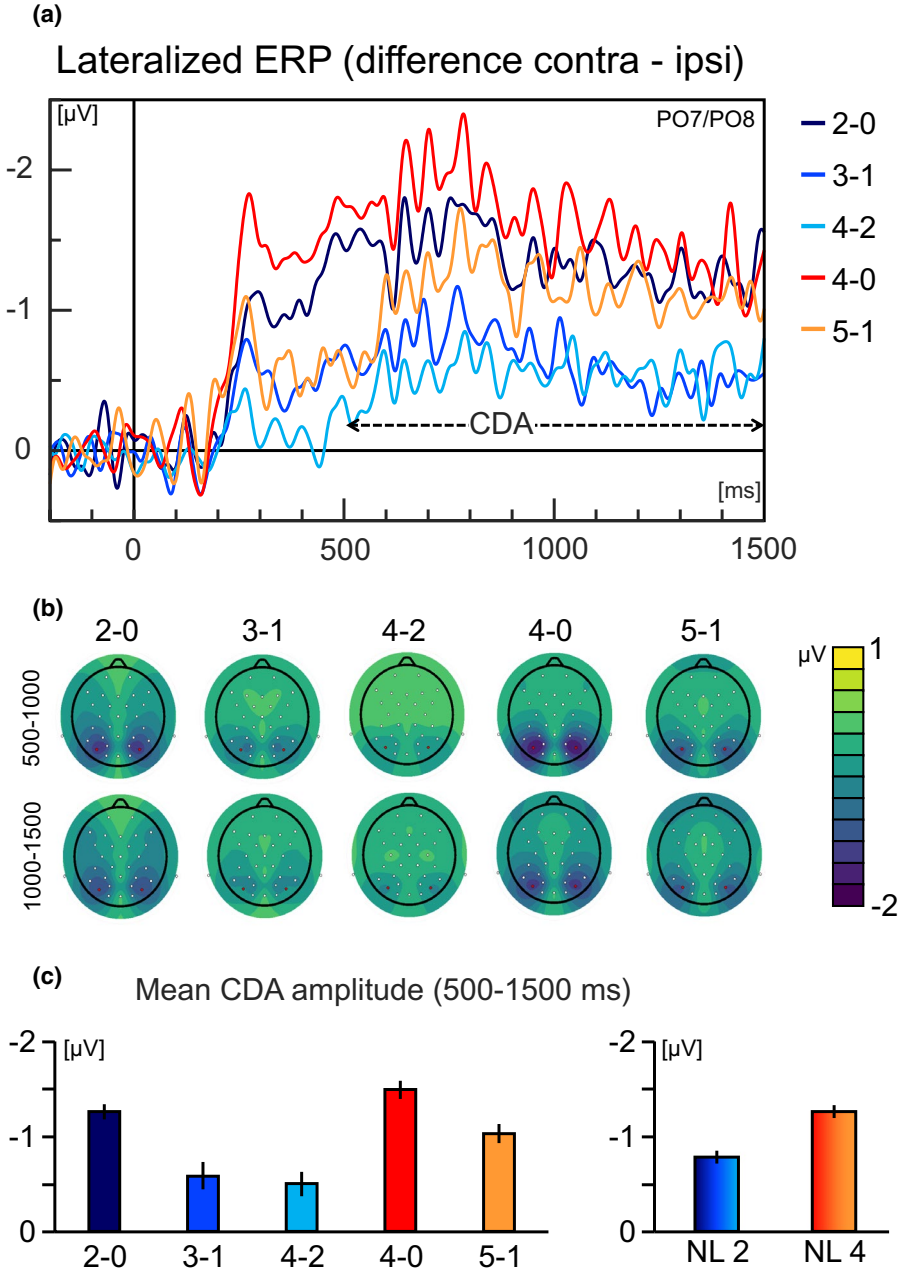

FIGURE 4 (a) Grand average lateralized waveforms (contra—ipsi, relative to the high-load hemifield, averaged across PO7/PO8, separately for all lateralized target distributions. Conditions with net load 2 are in shades of blue, conditions with a net load of 4 in shades of red. For statistical analyses of CDA, the unfiltered average amplitude from 500–1,500 ms was used. For illustration purposes, waveforms shown here were low-pass filtered (non-causal Butterworth low-pass filter, half-amplitude cutoff = 30 Hz, slope = 24 dB/octave). (b) Topography of the average activity at each electrode site from 500–1,000 ms (upper row) and from 1,000–1,500 ms (lower row), red electrodes indicate PO7/PO8. Note that topographies are perfectly symmetrical because values were averaged across paired electrodes (c) Mean CDA amplitude from 500–1,500 ms, separately for each lateralized target distribution and separately for net load (NL) 2 and 4. Error bars denote standard errors of the mean, corrected for within-subjects comparisons (Cousineau, 2005)

3.4 | Analyses separately for sites contralateral to high-load and low-load hemifield (see Figure 5)

3.4.1 | Conditions separately

Mean amplitude for all lateralized conditions (=unequal target distributions), separately for the EEG signal contralateral to high-load and low-load hemifield can be found in Figure 5. Statistical analyses for pairwise comparisons can be found in Table 1. Note that "contralateral to low-load hemifield" is tantamount to "ipsilateral to high-load hemifield" the difference which constitutes the CDA as reported above. A 1 × 5 ANOVA demonstrated that mean amplitude contralateral to the high-load hemifield varied as a function of target distribution, $F(4,80) = 3.4$, $p = .013$, and $\eta^2 = .14$. Similarly, the

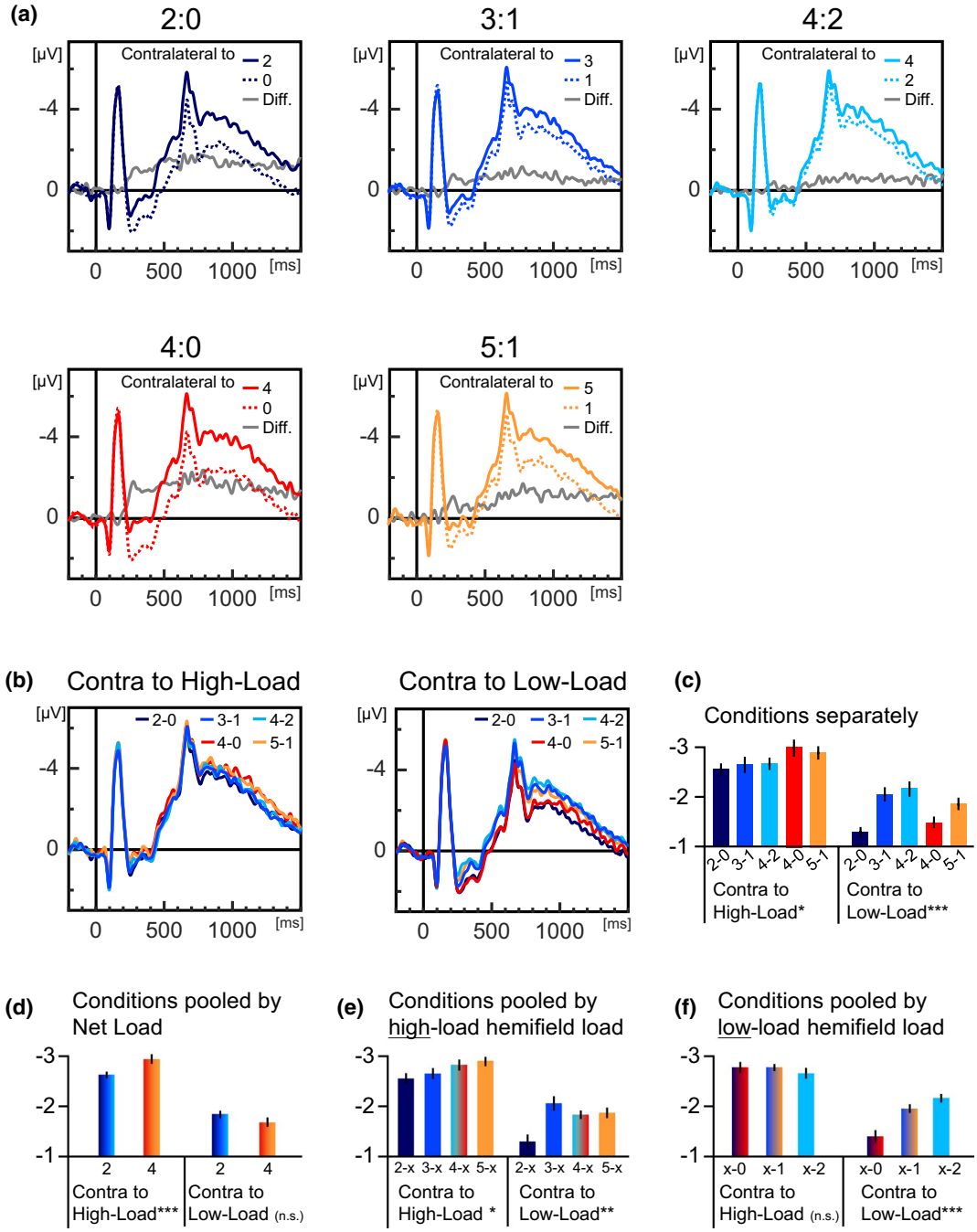

FIGURE 5 (a) Grand average waveforms for electrodes PO7/PO8 contralateral to high-load hemifield (solid colored lines) and low-load hemifield (stroked colored lines), each panel showing one of the lateralized target distribution condition. Gray lines show the difference waveforms (high-load—low-load) and are identical to the CDA waveforms in Figure 3a. The same waveforms as in (A) are shown grouped by high-load and low-load hemifield in (b), and their mean amplitude (500–1,500 ms) in (c). The same mean electrode as in (C) is shown pooled by net load (d), high-load hemifield load (e) and low-load hemifield (f). Indicators of statistical significance (*ns* = not significant, **p* < .05, ***p* < .01, ****p* < .001) refer to statistical tests comparing conditions separately for activity contralateral to high-load and low-load hemifield (see text for details). For illustration purposes, all waveforms shown here were low-pass filtered (non-causal Butterworth low-pass filter, half-amplitude cutoff = 30 Hz, slope = 24 dB/octave). Error bars denote standard errors of the mean, corrected for within-subjects comparisons (Cousineau, 2005)

mean amplitude contralateral to the low-load hemifield varied as a function of target distribution $F(4,80) = 9.4$, $p < .001$, and $\eta^2 = .32$. It is noteworthy that for the EEG signal contralateral to the high-load hemifield, none of the pairwise comparisons *within* net load (see column "comparison" in Table 1) were significant (all $p \geq .248$), whereas all comparisons *between* net loads were significant (all $p \leq .048$) except for 4-2 versus 5-1 that was marginally significant ($p = .065$).

TABLE 1 Statistical analyses comparing lateralized conditions, separately for EEG signal contralateral to high-load and low-load hemifield

Conditions separately					
Contralateral to …	**Comparison**	**Conditions**	***t*(20)**	***p***	**Cohen's *d***
High-load hemifield	Within net load	2-0 vs. 3-1	0.6	.290	0.12
		2-0 vs. 4-2	0.6	.283	0.13
		3-1 vs. 4-2	0.2	.440	0.03
		4-0 vs. 5-1	0.7	.246	0.15
	Between net loads	2-0 vs. 4-0	3.1	**.003**	0.68
		2-0 vs. 5-1	3.3	**.002**	0.71
		3-1 vs. 4-0	3.0	**.004**	0.65
		3-1 vs. 5-1	1.7	**.048**	0.38
		4-2 vs. 4-0	2.3	**.018**	0.49
		4-2 vs. 5-1	1.6	.065	0.34
Low-load hemifield	Within low-load hemifield load	2-0 vs. 4-0	1.2	.118	0.27
		3-1 vs. 5-1	1.0	.168	0.22
	Between low-load hemifield loads	2-0 vs. 3-1	3.4	**.001**	0.75
		2-0 vs. 5-1	3.8	**.001**	0.83
		2-0 vs. 4-2	5.4	**.000**	1.19
		3-1 vs. 4-0	2.7	**.007**	0.59
		4-0 vs. 5-1	3.5	**.001**	0.77
		4-2 vs. 4-0	4.2	**.000**	0.92
		3-1 vs. 4-2	0.6	.287	0.12
		4-2 vs. 5-1	2.7	**.007**	0.58
Conditions pooled by load in high-load hemifield					
Contralateral to …		**Conditions**	***t*(20)**	***p***	**Cohen's *d***
High-load hemifield		2-x vs. 3-x	0.6	.290	0.12
		2-x vs. 4-x	1.8	**.040**	0.40
		2-x vs. 5-x	3.3	**.002**	0.71
		3-x vs. 4-x	1.9	**.039**	0.41
		3-x vs. 5-x	1.7	**.048**	0.38
		4-x vs. 5-x	0.6	.285	0.13
Low-load hemifield		2-x vs. 3-x	3.4	**.001**	0.75
		2-x vs. 4-x	3.8	**.001**	0.84
		2-x vs. 5-x	3.8	**.001**	0.83
		3-x vs. 4-x	1.2	.114	0.27
		3-x vs. 5-x	1.0	.168	0.22
		4-x vs. 5-x	0.4	.336	0.09
Conditions pooled by load in low-load hemifield					
Contralateral to …		**Conditions**	***t*(20)**	***p***	**Cohen's *d***
High-load hemifield		x-0 vs. x-1	0.0	.488	0.01
		x-0 vs. x-2	0.7	.238	0.16
		x-1 vs. x-2	0.9	.186	0.20
Low-load hemifield		x-0 vs. x-1	4.6	**.000**	1.01
		x-0 vs. x-2	5.6	**.000**	1.22
		x-1 vs. x-2	1.7	0.052	0.37

Bold values are significant.

For the EEG signal contralateral to the low-load hemifield, a different pattern was found. Here, none of the comparisons within low-load hemifield load (= number of targets in hemifield with fewer targets) were significant (both $p \geq .118$), whereas all comparisons between low-load hemifield loads (all $p \leq .007$) except for 3-1 versus 4-2 ($p = .287$) were significant. Thus, contralateral activity to high-load hemifield was mainly determined by net load, whereas contralateral activity to low-load hemifield was mainly determined by the number of targets in the low-load hemifield. The low-load hemifield load effect was analyzed in combination with the high-load hemifield load (see below). The net load effect was confirmed with a 2 × 2 ANOVA with the within-subjects factors Laterality (contralateral to high-load vs. low-load hemifield) and net load (2 versus. 4), $F(1,20) = 13.8$, $p = .001$, and $\eta^2 = .41$. Follow-up t tests for dependent measures showed that for the signal contralateral to the high-load hemifield, net load 4 was more negative than net load 2, $t(20) = 4.5$, $p < .001$, and $d = 0.98$, whereas for the signal contralateral to the low-load hemifield, net load 2 and net load 4 were similar in amplitude, $t(20) = 1.4$, $p = .086$, and $d = 0.31$.

3.4.2 | Conditions pooled

As net load is determined by the number of targets in both hemifields, follow-up analyses scrutinized the contribution of high-load and low-load in separate analyses. To this end, the signal contralateral to the high-load hemifield and the signal contralateral to low-load hemifield were pooled by (a) high-load hemifield load (Figure 5d, middle rows in Table 1) and (b) low-load hemifield load (Figure 5e, bottom rows in Table 1). For example, the 4-2 and 4-0 conditions were pooled to represent four targets (4-x) in the high-load hemifield and the 3-1 and 5-1 conditions were pooled to represent one target (x-1) in the low-load hemifield. The signal contralateral to high-load hemifield varied as a function of high-load hemifield load ($F(3,60) = 2.9$, $p = .041$, and $\eta^2 = .13$) and showed a linear ($p = .002$) but not a quadratic or cubic trend (both $p \geq .488$). This was driven by a monotonically increasing negativity with high-load hemifield load with all direct comparisons being reliable (all $p \leq .048$) except for 2-x versus 3-x ($p = .290$) and 4-x versus 5-x ($p = .285$). The signal contralateral to low-load hemifield also varied as a function of number of items in the high-load hemifield ($F(3,60) = 7.6$, $p = .002$, and $\eta^2 = .27$) and showed a linear, quadratic, and cubic trend (all $p \leq .036$). This was driven by the 2-x conditions showing significantly smaller amplitudes compared to all other conditions (all $p \leq .001$), whereas 3-x, 4-x, and 5-x did not differ among each other (all $p \geq .114$). The signal contralateral to high-load hemifield did not vary as a function of low-load hemifield load ($F(2,40) = 0.5$, $p = .531$, and $\eta^2 = .03$). This was evident in none of the low-load hemifield load conditions deviating from one another reliably (all $p \geq .186$). The signal contralateral to the low-load hemifield, however, varied as a function of low-load hemifield load ($F(2,40) = 19.4$, $p < .001$, and $\eta^2 = .49$) and shows a linear ($p < .001$) but not a quadratic trend ($p = .091$). This was driven by a low-load hemifield load of x-0 being reliably smaller than x-1 and x-2 (both $p < .001$) and a low load hemifield load of x-1 being marginally smaller than x-2 ($p = .053$). These results show that the signal contralateral to the high-load hemifield is mainly driven by the number of targets in the high-load hemifield, which explains the net load effect described above. In addition, the signal contralateral to the low-load hemifield is mainly driven by the number of targets in the low-load hemifield.

3.5 | Modeling the net CDA

The lateralized ERP results indicate that the CDA amplitude varied within each net load condition. For example, the CDA was larger in the 4-0 than in the 5-1 condition. The CDA amplitude of an ideal observer (with K ≥ 6) should closely reflect the net load, for example, be of equal size for the 4-0 and the 5-1 conditions as they could encode all items. The varying CDA amplitudes in the present data may not be surprising, however, given that participants' working memory capacity was lower than set size most conditions (mean K = 2.5). Accordingly, a participant with a capacity of 3 may have encoded three items from one hemifield in the 4-0 condition, resulting in a encoding imbalance (the "real net load") of 3. The same participants may have encoded two items from one hemifield and one from the other hemifield in the 5-1 condition, resulting in a encoding imbalance of 1. The CDA amplitude should depend on the encoding imbalance, that is, the imbalanced resulting from which items were actually encoded. The observed CDA amplitudes could thus reveal how the visual system samples items from the visual environment to be encoded into working memory.

This was tested with a model. In its most simple form ($\omega = 1$), the model assumed that all target items on the screen were equally likely encoded into working memory. For example, a participant with a working memory capacity of K = 3 would randomly pick three out of six items in the 4-2 condition which means that on average they should have an encoding imbalance of one item ($4/6 - 2/6 \times 3 = 1$; i.e., participants encode one more item from the hemifield with four target than from the hemifield with two targets). In the 5-1 condition, the predicted encoding imbalance is 2 ($5/6 - 1/6 \times 3 = 2$) and in the 3-1 condition, the encoding imbalance should be 1.5 ($3/4 - 1/4 \times 3 = 1.5$) targets on average. An additional model parameter was the weight of items

in the hemifield with more items. While for ω = 1, that is, each item was equally likely sampled, this weight could also be smaller or larger than 1. A weight of ω = 1.1, for example, would mean that all items from the low-load hemifield have an increased chance of 10% to be encoded into working memory (with all items from the high-load hemifield having a combined decreased chance of 10%). The model assumed that the weight would be identical for all participants.

In a first step, the expected average encoding imbalance was calculated for each participant and each of the five lateralized conditions, taking an individual's working memory capacity into account and varying weights from 0.5 to 2.0 in steps of 0.001. In a second step the *expected* encoding imbalance was compared with the *measured* CDA in each condition. More precisely, we estimated a standard one-item-CDA amplitude by dividing the observed CDA in each condition by the expected encoding imbalance. In the above mentioned example of an individual with K = 3 and ω = 1, the CDA in the 4-2 condition divided by 1, the CDA in the 5-1 condition divided by 2, and the CDA in the 3-1 condition divided by 1.5 should be similar as the resulting amplitudes should each reflect an imbalance of one item. If a given weight was reflecting the encoding bias across participants well, the resulting estimated one-item-CDA amplitudes should be similar. The standard deviation of the estimated one-item-CDA amplitudes were taken as a measure of model fitness. The model was run for the average CDA amplitude from 500 to 1,500 ms.

The weight that resulted in the lowest standard deviation of the five estimated CDA amplitudes was determined as ω = 1.064. To statistically evaluate whether the estimated one-item CDA amplitudes were indeed identical, they were first forwarded to a 1 × 5 ANOVA for repeated measures,

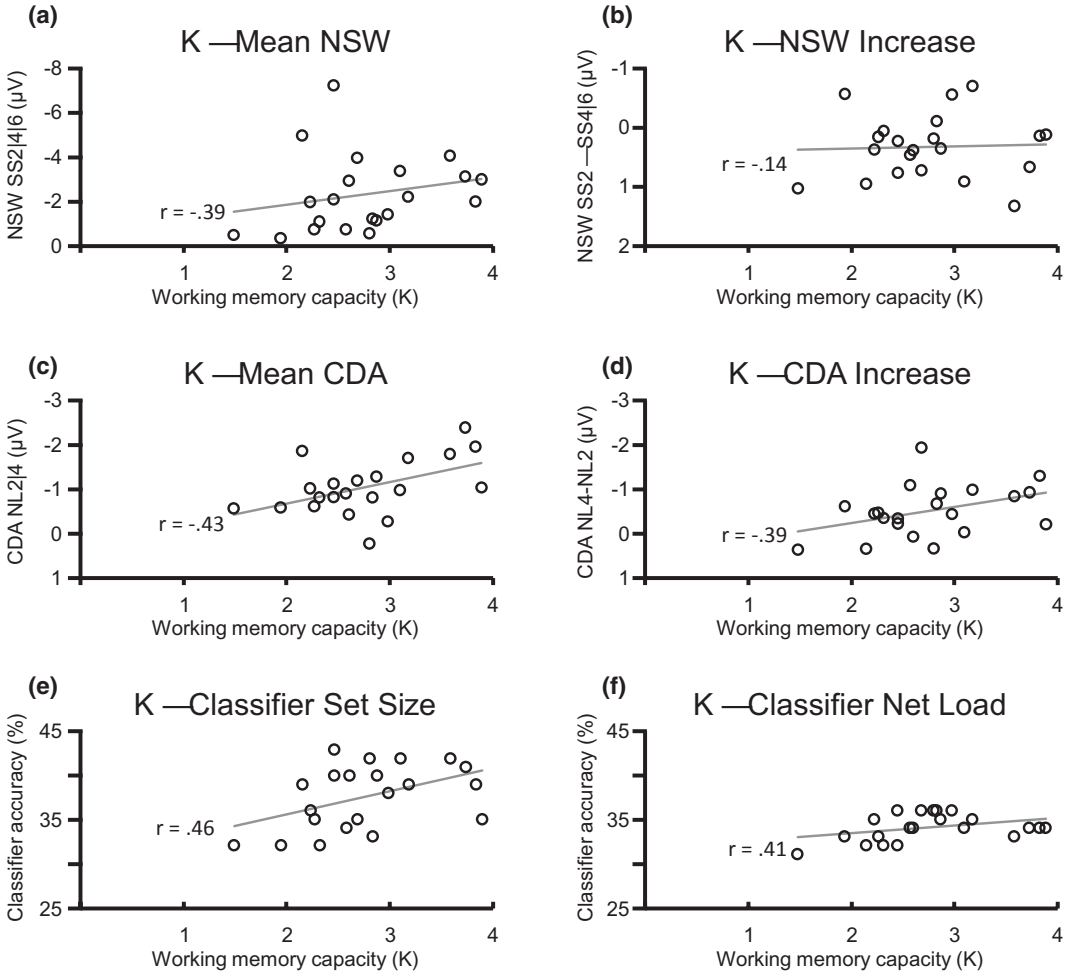

FIGURE 6 Scatterplot of working memory capacity K and (a) mean Negative Slow Wave (NSW), averaged across set size 2, 4, and 6, (b) NSW increase (mean NSW amplitude for SS 4 and 6 minus NSW amplitude for SS 2), (c) mean contralateral delay activity (CDA), averaged across net load 2 and 4, (d) CDA increase (CDA amplitude for net load 4 minus CDA amplitude for net load 2), (e), set size classification accuracy, (f), net load classification accuracy. Gray lines show linear trend and r refers to Spearman's rho (note that slope of gray line and r do not perfectly match because r indicates rank correlation coefficient). For A-D, a negative correlation denotes a positive relationship between K and the respective measure as the measure itself has a negative sign (e.g., CDA has a negative amplitude)

showing no reliable effect of net load ($F(4,80) = 0.3$, $p = .695$, and $\eta^2 = .02$). In addition, t tests for dependent measures were run to compare the estimated CDA amplitude for all net load conditions pair-wise. All 10 comparisons had a $p \geq .121$, demonstrating that the model explained the observed CDA reasonably well. The results suggest that individuals sample targets from the visual field with a 6.4% increased chance from the hemifield with fewer targets. The CDA amplitude was a result of this stochastic imbalance between the hemifields, moderated by an individual's working memory capacity.

3.6 | Decoding Accuracy (see Figure 6)

Decoding accuracy for set size was higher than for shuffled set size, $t(20) = 5.3$, $p < .001$, and $d = 1.16$. Decoding accuracy for net load was higher than for shuffled net load, $t(20) = 2.0$, $p = .028$, and $d = 0.44$. The first time period for which at least three consecutive time bins (i.e., 15 ms) were reliably different from shuffled data started at 185 ms for set size and at 305 ms for net load (see red lines in Figure 6).

3.7 | Correlations (see Figure 7)

K correlated with NSW ($r = -.39$, $p = .042$) and with CDA ($r = -.43$, $p = .026$), demonstrating that both a larger (more negative) NSW amplitude and a larger (more negative contralateral than ipsilateral) CDA amplitude predicted a high working memory capacity. K also correlated with CDA increment ($r = -.39$, $p = .040$), demonstrating that the more CDA amplitude increased with net load, the higher an individual's working memory capacity. K did not correlate with NSW increment ($r = -.14$, $p = .260$). Moreover, K correlated with the set size classifier ($r = .46$, $p = .018$) as well as the net load classifier ($r = .41$, $p = .032$). A linear regression model showed that ERP measures (CDA, CDA increase, NSW, NSW increase) accounted for 31.2% of the variance of K. Classification measures (set size and net load classification accuracy) accounted for 30.1% of the variance

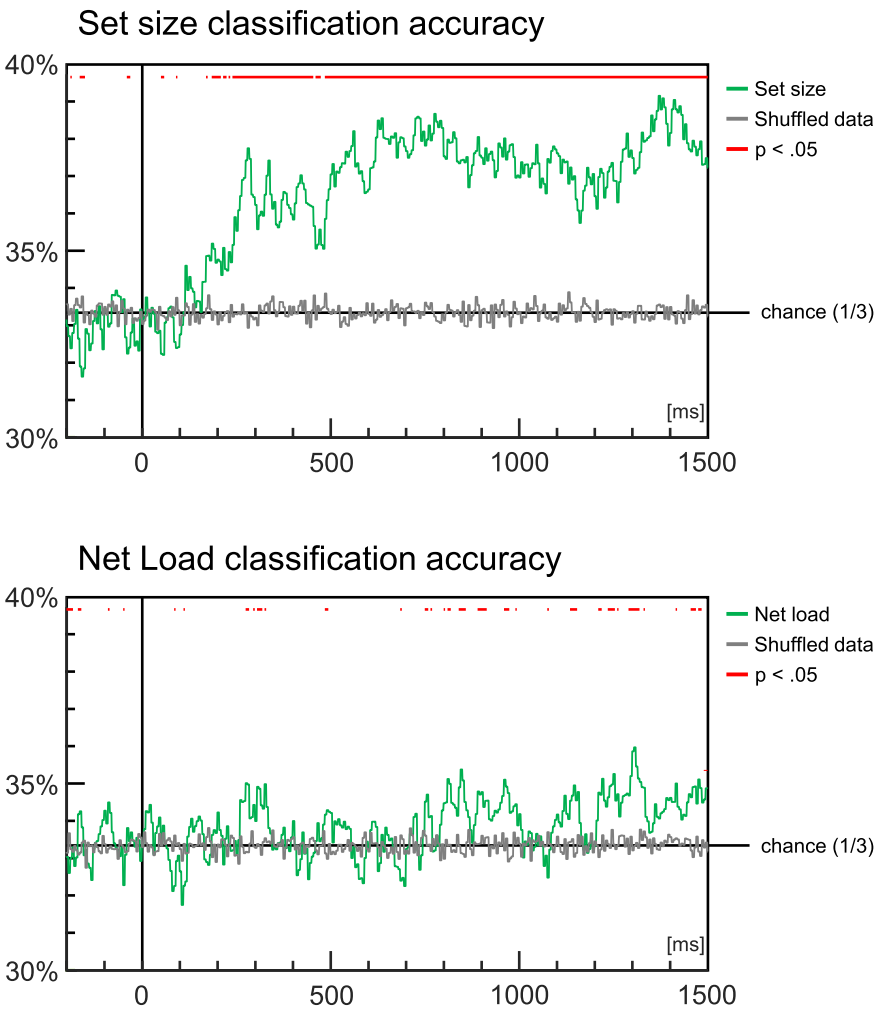

FIGURE 7 Green lines show classification accuracy for set size (upper row) and net load (lower row). Trained on 2/3 of trials, tested on the remaining 1/3. Gray lines show classification accuracy of shuffled data (random assignment of set size or let load labels to trials) as a control. Red lines indicate time points where t tests for dependent measures (one-tailed) showed a reliable difference between classification accuracy for real data and shuffled data. As there were three set sizes and three net loads, classification chance level was 1/3 (black horizontal line)

of K. All measures combined accounted for 58.6% of the variance of K.

4 | DISCUSSION

This study presents a novel change detection paradigm that allows to simultaneously measure the CDA and the NSW as measures of working memory. They first key finding of the present study was that the NSW increased with set size (i.e., number of targets) when the total number of items (targets and distractors) and thus overall physical stimulation was kept constant. The second key finding was that a CDA was observed without cueing participants to either hemifield; the CDA varied as a function of the imbalance of items memorized from the left versus right hemifield. Third, the lateralized EEG signal was mostly determined by the number of items in the contralateral hemifield. Fourth, participants encoded items into working memory more balanced (biased away from the hemifield with more items) as random sampling would predict. Fifth, a linear classifier could decode set size (and to some extent, net load) from the raw (unfiltered) EEG signal. Sixth, NSW, CDA, and classifier accuracy were good predictors of working memory capacity highlighting their functional significance as neural markers of working memory.

4.1 | The NSW as a measure of set size

Participants were presented with 12 stimuli, six in each hemifield, in every trial. They had to maintain targets (colored circles) in working memory while ignoring distractors (colored squares). The number of targets (set size of 2, 4, or 6) and the imbalance between hemispheres (net load 0, 2, or 4) was varied. Replicating earlier studies, NSW increased with set size (Bailey, Mlynarczyk, & West, 2016; McEvoy, 1998; Ruchkin et al., 1992) and asymptoted for supra-capacity set sizes (Fukuda et al., 2015). In the present study, an overall working memory capacity of K = 2.5 (K = 2.8 excluding sub-capacity set size trials) was measured and the NSW did not increase from set size 4 to 6, presumably because the working memory capacity was already depleted with four memorized items for most participants. NSW amplitude predicted working memory capacity, demonstrating its functional significance: The larger an individual's capacity, the more pronounced was the NSW. As opposed to previous studies, the total number of items (set size + number of distractors) was kept constant, ruling out the possibility that the overall physical stimulation can account for the set size effect. This comes with another confound, however, namely the number of distractors. In the present study, 10 distractors were presented in the set size 2 condition, eight distractors in the set size 4 condition, and six distractors in the set size 6 condition. However, as the NSW was found to *increase* with cognitive demands (Zickerick et al., 2020) and amount of filtering needs (Schneider et al., 2017), a *decreased* number of distractors in the high-load conditions seems unlikely as a reason for an increased NSW amplitude. As it is impossible to control for both total number of items and number of distractors while varying the number of targets, the paradigm presented here and the traditional NSW paradigm without distractors (e.g., Fukuda et al., 2015) constitute complementary approaches to non-lateralized neural measures of working memory.

The advantage of the present paradigm is that in addition to the NSW, the CDA as a lateralized neural correlate of working memory can be measured in the same trials (see next paragraph). NSW did not only vary with set size, but also with net load. In contrast to the CDA, NSW decreased with net load. The maximum NSW amplitude for net load 0 may be related to the bilateral field advantage, that is, the preference to encode items equally from both hemifields (see below). However, as paradigms measuring the NSW do not typically vary net load, this remains speculative and the functional significance of this effect has yet to be scrutinized.

4.2 | The CDA as a measure of net load

In order to induce a spatial imbalance in working memory, change detection tasks typically employ lateralized designs: participants are presented with stimuli in both hemifields but are asked to only encode items from the cued hemifield (Fukuda, Kang, & Woodman, 2016; Luria et al., 2016; Vogel & Machizawa, 2004). The CDA is then observed as a negativity at sites contralateral to the relevant hemifield, compared to ipsilateral sites. A CDA is, however, also observed without cues when a spatial imbalance is inherent of the target distribution (Berggren & Eimer, 2016; Feldmann-Wüstefeld et al., 2019; Feldmann-Wüstefeld & Vogel, 2018; Jolicœur et al., 2008; Töllner et al., 2013). In the current study, the difference in number of targets between the left and right hemifield, the net load, determined the CDA amplitude. A net load of 4 produced a larger CDA than a net load of 2. As the total number of stimuli was identical in both hemifields, the CDA amplitude difference cannot be explained by differences in bottom-up processes. The present study shows that the well-established effect of working memory load on CDA amplitude (Drew & Vogel, 2008; Ikkai, McCollough, & Vogel, 2010; Jolicœur et al., 2008; Luria et al., 2016; Salahub & Emrich, 2018; Vogel et al., 2005) can be replicated without the use of spatial cues. Furthermore, both CDA amplitude and CDA increase (from net load 2 to 4) predicted working memory capacity K, replicating earlier studies

(Luria et al., 2016; Vogel et al., 2005). CDA amplitude was generally higher and increased more for those individuals that could, on average, store more items in working memory. This highlights the functional significance of the target-imbalance-induced CDA as a measure of working memory load. Thus the present study shows that a "cue-less" change detection task shares crucial properties with the traditional change detection task and may be used interchangeably.

A potential advantage of the cue-less design may be that cue-induced attention processes that can complicate the interpretation of results do not need to be considered. For example, attention deployment prior to memoranda onset could affect the working memory manipulation of a research question at hand or directing attention to the wrong hemifield may affect working memory efficiency. Furthermore, cue properties themselves can affect neural measures of working memory (Cooreman et al., 2015; Herrero et al., 2009; Wiegand et al., 2018). Importantly, the present paradigm lets participants focus on one simple task ("remember all circles") and thus avoids a dual-task situation that is imposed on participants when they have to both attend a hemifield according to a cue and to encode items into working memory (Sander et al., 2011). This may be particularly helpful when comparing groups that could be differentially affected by attentionally demanding tasks, for example, young and older adults or psychiatric patients and a control group. Related to this, a further practical implication of the new task is that experimental runtime may be overall shorter. The present task is easier to explain and practice, eye movements may be reduced as both hemispheres have to be attended, and each trial is reduced by the duration of the cueing interval. It was argued that the CDA measured in traditional lateralized designs may not only reflect the number of targets in the cued hemifield but also the number of distractors in the uncued hemifield (Fukuda et al., 2015; Sauseng et al., 2009) that are required to proportionally increase with set size in order to achieve physical balance in both hemifields. The present paradigm circumvents this problem by keeping the number of items constant in both hemifields. This means the larger amplitude in the 5-1 than in the 3-1 condition cannot be due to the number of contralateral distractors (there are five distractors in the hemifield with one target in each case).

4.3 | How do individuals sample targets from both hemifields into working memory?

A potential caveat of the present design is that for supra-capacity set size displays, the CDA amplitude may vary as a function of the specific target distribution in the left and right hemifield and how participants sample targets. For example, in the present study, a 3-1 distribution produced a larger CDA than a 4-2 distribution, inducing variability within the net load 2 condition. Then again, such variations within a given net load can also be meaningful in a way that they can reveal how items are encoded into working memory.

Here, the observed CDA amplitude variations could be explained by a stochastic process of selecting items for encoding into working memory. If an ideal observer with a capacity $K \geq 6$ encoded items randomly from a 3-1 and 4-2 display, the elicited CDA amplitude should be identical. If, however, an individual with $K < 6$ encoded items randomly from a 3-1 and 4-2 display, with equal probability for each item, 3-1 displays would elicit a larger CDA than 4-2 displays. This is because the average or expected encoding imbalance (the *actual* net load) would be different for 3-1 than for 4-2. How imbalanced the encoding imbalance was in the present study depended on an individual's working memory capacity. A model taking each participant's working memory capacity into account showed a low-load hemifield weight of 1.064, that is, a 6.4% increased chance for items from the low-load hemifield to be encoded. Interestingly, this is close to the behavioral advantage for items from the low-load hemifield (5.8%). A recent study showed that for two sequentially presented groups of targets, the first and second group are equally strongly represented in working memory (Feldmann-Wüstefeld et al., 2018). The present study shows that within one group of targets, the weight can vary, namely as a function of the relative spatial distribution. As a result of more likely encoding from the low-load hemifield, the overall encoding is *more* balanced than one would expect if encoding was entirely random.

This tendency to achieve spatial encoding balance is in line with the bilateral field advantage. The bilateral field advantage is based on the assumption that the ability to simultaneously process multiple items is limited by the extent to which those items are represented by nonoverlapping neural representations (Cohen, Konkle, Rhee, Nakayama, & Alvarez, 2014; see also Awh & Pashler, 2000). As a result, working memory performance is better for items that are distributed across hemifields compared to presented in the same hemifield (Alvarez & Cavanagh, 2005; Cohen et al., 2014; Holt & Delvenne, 2015). The overall tendency toward a more balanced encoding observed here means that the targets' neural representations overlap less. While previous studies assessing a bilateral field advantage typically forced participants to encode targets from both versus one hemifield., in the present experiment participants could decide which (if any) hemifield to preferably encode from (except for conditions 2-0 and 4-0). Thus it is not clear if the increased weight for low-load hemifields is a deliberate strategy or a more general bias inherent in the visual system. Future research could explore these possibilities and determine the selection mechanism in more detail. This could be done, for example, using

post-experimental questionnaires asking participants for their strategies (van Lamsweerde & Beck, 2011) or by inducing a preference to one or the other hemifield through cues (Zhang & Luck, 2008) or incentives (Klyszejko, Rahmati, & Curtis, 2014). Alternatively, a whole-report change detection task could be used that probes each item in the visual field and thus allows to determine the working memory accuracy for all items in the visual field (Adam, Vogel, & Awh, 2017), providing a more direct measure for encoding strategies in unbalanced displays.

4.4 | Contra- and ipsilateral activity as hemifield-specific neural measures of working memory

If the CDA is only analyzed as the differential contra- and ipsilateral activity, the specific responses to each hemifield may go unnoticed even though they can carry relevant information. For example, previous studies demonstrated that when targets are presented in one hemifield and distractors in the other, the EEG signal contralateral to the targets is mostly affected by the targets (Arend & Zimmer, 2011; Liesefeld et al., 2014). For particularly low memory loads, however, the EEG signal contralateral to the target is also affected by the number of distractors (Arend & Zimmer, 2011), possibly because leftover working memory capacity is automatically used for distractors (Lavie, 2005, see also Vogel et al., 2005).

In contrast to previous studies using lateralized change detection tasks, targets were presented in both hemifields in the present study. Thus a distinction between contra- and ipsilateral needs to be considered relative to either the high-load hemifield (hemifield with more numerous targets) or the low-load hemifield (with fewer targets). First, the present results confirmed earlier studies (Arend & Zimmer, 2011; Liesefeld et al., 2014) and also demonstrated that activity in either hemisphere is mostly determined by the number of targets in the opposite hemifield. The signal contralateral to the high-load hemifield increased with the number of targets in that hemifield, but remained unaffected by the number of targets in the low-load hemifield. The signal contralateral to the low-load hemifield also increased with the number of targets in that hemifield. The signal contralateral to the low-load hemifield was, however, also affected by the number of items in the high-load hemifield. It is likely that this was an experimental artifact: The signal contralateral to the low-load hemifield was not affected by the high-load hemifield when the average number of targets in the low-load hemifield was constant (3-x, 4-x, or 5-x conditions had an average of one target in the low-load hemifield), but was considerably smaller when the number of targets in the low-load hemifield was lower than 1 (the 2-x condition had 0 targets in the low-load hemifield). This is not surprising as 0 targets are expected to elicit a small lateralization. The fact that any lateralization was found in the 2-0 (as well as in the 4-0) condition, suggests that distractors were erroneously encoded into working memory, at least in some trials, replicating earlier studies (Arend & Zimmer, 2011). Thus, in a nutshell, the present results suggest that the lateralized EEG signal is determined by the number of targets in the contralateral hemifield.

Single-hemispheric activity can be considered a valid neural measure of hemifield-specific working memory load and may be particularly useful for experimental designs that aim at measuring competition between items for working memory slots directly. For example, future studies could associate items from one hemifield with a higher reward than items from the other hemifield to induce a higher priority (Heuer & Schubö, 2018; Reinhart & Woodman, 2014) or simple items could be presented in one hemifield and complex items in the other hemifield (Balaban & Luria, 2015b; Brady, Störmer, & Alvarez, 2016). The contralateral activity to each hemifield should then isolate the processing of the respective items, compare processing and pinpoint competition.

4.5 | Decoding working memory load and load imbalance

The present study also investigated whether set size and net load could be decoded from EEG data using an information-based decoding approach. The information-based decoding approach is a multivariate measure of the information content present in the neural signals of each individual participant and can be used to quantify cognitive processes (Bae et al., 2020). Here, separate linear classifiers were trained for each participant on 2/3 of the trials to decode the given set size or net load as accurately as possible. The classifier was then tested in the remaining 1/3 of the trials, for bins of 5 ms to track decoding accuracy in a time-resolved manner. Using unfiltered (raw) EEG data, the classifier could decode set size reliably from 185 ms on, a time window that precedes working memory processes and is typically associated with attentional processes (Jolicœur et al., 2008). In line with the notion that decoding accuracy of working memory content reflects the maintenance of relevant information in working memory (Bae & Luck, 2019; Foster et al., 2016), decoding accuracy remained above chance throughout the retention interval. Decoding the load imbalance (net load) was less reliable; although the classification accuracy was significant when the entire time window (500–1,500 ms) was used, time bin by time bin analyses only show occasional intervals of reliable classification accuracy throughout the entire retention interval. The first cluster of reliable net load classification accuracy was found at 305 ms. Both raw EEG data (Bae &

Luck, 2019) and alpha-band activity (Foster et al., 2016) have recently been shown to allow decoding working memory content, but these studies have decoded target *identity* or *location,* whereas the current study demonstrates that working memory *load* as well as *load imbalance* can be decoded as well (for another recent demonstration of set size decoding, see Adam et al., 2020). As up to six targets were shown at random positions in the current study, decoding either identity or location as a comparison to decoding working memory load is not feasible here. Future research, however, should compare how well different features, spatial attributes or working memory load can be decoded and which functional significance they may have.

Again, the number of total items (targets + distractors) was kept constant in the present study which means that the classifier did not just pick up on bottom-up differences but presumably reflected the "cognitive imbalance", that is, it reflected the encoding of more or fewer targets. This might render "multivariate load detection" (Adam et al., 2020) a valuable tool to track cognitive processes. The functional significance of the classifier is evident in its correlation with working memory capacity. Classification accuracy predicted a participant's working memory capacity K, suggesting that varying set sizes induced more distinct brain activity patterns in high performers. Such a correlation was also found for a "net load decoder" based on raw EEG data. Participants with a high capacity showed a better net load decoding accuracy, suggesting that varying net loads induced more distinct brain activity patterns in participants with a high capacity. The classification accuracy could account for 30.1% of the variance of K, similar to NSW and CDA amplitude and amplitude increase that could account for 31.2% of the variance of K (out of 58.6% variance explained by all measures combined). This highlights the methodological significance of using information-based decoding approaches. Decoding accuracy for working memory content has recently been shown to differentiate between schizophrenic and non-schizophrenic individuals (Bae et al., 2020) and future research could apply this technique to other neuropsychiatric populations or use it as a tool in interindividual approaches.

4.6 | Conclusions and future directions

The change detection paradigm presented here requires participants to attend both hemifields. The *non-lateralized* signal showed that the amplitude of the NSW increased with the number of targets and predicted working memory capacity K, replicating earlier studies (Fukuda et al., 2015; Wiegand et al., 2014). As total stimulation was kept constant, the present paradigm shows that the set size dependent NSW amplitude previously observed was not due to physical confounds but reflects an increasing working memory load. The *lateralized* signal showed that activity in each hemisphere reflected the number of targets in the contralateral hemifield, replicating previous studies (Arend & Zimmer, 2011). Because targets were shown in both hemifields, a cue directing attention toward one hemifield was not necessary in the present study. Rather, an imbalance in target distribution across hemifields (net load) induced a "cognitive" lateralization. The target imbalance, that does not implicate physical imbalance as the total number of items was kept constant, elicited a CDA similar to traditional change detection tasks that use cues to direction attention to either hemifield (Luria et al., 2016; Vogel & Machizawa, 2004; Vogel et al., 2005). The CDA was measured in the same displays as the NSW. CDA amplitude increased with net load, particularly for individuals with a high working memory capacity. This is analog to how the CDA behaves in traditional change detection tasks (Vogel & Machizawa, 2004) and shows that the present paradigm is suitable to track individual differences in the neural signature of working memory. Within net load, the specific target distribution determined the CDA amplitude and revealed that participants encoded items preferably from the hemifield with fewer items. The encoding bias resulted in a more balanced encoding than random sampling would predict, in line with the notion of a bilateral advantage of working memory representations (Alvarez & Cavanagh, 2005). A linear classifier was able to decode set size. Decoding accuracy of the classifier increased with working memory capacity, showing that information-based decoding approaches can be useful to track individual differences in cognitive processes.

The neural measures used in the present study accounted for almost 60% of the variance in working memory capacity which demonstrates that a holistic approach can be useful when examining working memory processes. Future studies could use the paradigm presented here to provide converging evidence for a given hypothesis with an multitude of measures. For example, an experimental manipulation that reduces CDA amplitude, reduces NSW amplitude, and reduces decoding accuracy would be particularly compelling. At the same time, future studies could disentangle different aspects or sub-mechanisms of working memory by showing divergent patterns of working memory measures. For example, impairments in working memory through psychiatric disorders (Bae et al., 2020) or age-decline (Wiegand et al., 2014) may only be reflected in NSW amplitude, but not in CDA amplitude. Identifying double-dissociations among neural markers of working memory could be extremely useful in isolating more specific markers and examining working memory in a more fine-grained manner.

ORCID

Tobias Feldmann-Wüstefeld https://orcid.org/0000-0003-3189-7466

REFERENCES

Adam, K. C. S., Robison, M. K., & Vogel, E. K. (2018). Contralateral delay activity tracks fluctuations in working memory performance. *Journal of Cognitive Neuroscience*, *30*(9), 1229–1240. https://doi.org/10.1162/jocn_a_01233

Adam, K. C. S., Vogel, E. K., & Awh, E. (2017). Clear evidence for item limits in visual working memory. *Cognitive Psychology*, *97*, 79–97. https://doi.org/10.1016/j.cogpsych.2017.07.001

Adam, K. C. S., Vogel, E. K., & Awh, E. (2020). Multivariate analysis reveals a generalizable human electrophysiological signature of working memory load. *Neuroscience*. https://doi.org/10.1101/2020.06.04.135053

Alvarez, G. A., & Cavanagh, P. (2005). Independent resources for attentional tracking in the left and right visual hemifields. *Psychological Science*, *16*(8), 637–643. https://doi.org/10.1111/j.1467-9280.2005.01587.x

Arend, A. M., & Zimmer, H. D. (2011). What does ipsilateral delay activity reflect? Inferences from slow potentials in a lateralized visual working memory task. *Journal of Cognitive Neuroscience*, *23*(12), 4048–4056. https://doi.org/10.1162/jocn_a_00068

Awh, E., & Pashler, H. (2000). Evidence for split attentional foci. *Journal of Experimental Psychology: Human Perception and Performance*, *26*(2), 834–846. https://doi.org/10.1037/0096-1523.26.2.834

Baddeley, A. (2003). Working memory: Looking back and looking forward. *Nature Reviews Neuroscience*, *4*(10), 829–839. https://doi.org/10.1038/nrn1201

Bae, G.-Y., Leonard, C. J., Hahn, B., Gold, J. M., & Luck, S. J. (2020). Assessing the information content of ERP signals in schizophrenia using multivariate decoding methods. *NeuroImage: Clinical*, *25*, 102179. https://doi.org/10.1016/j.nicl.2020.102179

Bae, G.-Y., & Luck, S. J. (2018). Dissociable decoding of spatial attention and working memory from EEG oscillations and sustained potentials. *The Journal of Neuroscience*, *38*(2), 409–422. https://doi.org/10.1523/JNEUROSCI.2860-17.2017

Bae, G.-Y., & Luck, S. J. (2019). Reactivation of Previous Experiences in a Working Memory Task. *Psychological Science*, *30*(4), 587–595. https://doi.org/10.1177/0956797619830398

Bailey, K., Mlynarczyk, G., & West, R. (2016). Slow wave activity related to working memory maintenance in the N-back task. *Journal of Psychophysiology*, *30*(4), 141–154. https://doi.org/10.1027/0269-8803/a000164

Balaban, H., & Luria, R. (2015a). Integration of distinct objects in visual working memory depends on strong objecthood cues even for different-dimension conjunctions. *Cerebral Cortex*, *26*(5), 2093–2104. https://doi.org/10.1093/cercor/bhv038

Balaban, H., & Luria, R. (2015b). The number of objects determines visual working memory capacity allocation for complex items. *NeuroImage*, *119*, 54–62. https://doi.org/10.1016/j.neuroimage.2015.06.051

Berggren, N., & Eimer, M. (2016). Does contralateral delay activity reflect working memory storage or the current focus of spatial attention within visual working memory? *Journal of Cognitive Neuroscience*, *28*(12), 2003–2020. https://doi.org/10.1162/jocn_a_01019

Bigdely-Shamlo, N., Vankov, A., Ramirez, R. R., & Makeig, S. (2008). Brain activity-based image classification from rapid serial visual presentation. *IEEE Transactions on Neural Systems and Rehabilitation Engineering*, *16*(5), 432–441. https://doi.org/10.1109/TNSRE.2008.2003381

Brady, T. F., Störmer, V. S., & Alvarez, G. A. (2016). Working memory is not fixed-capacity: More active storage capacity for real-world objects than for simple stimuli. *Proceedings of the National Academy of Sciences*, *113*(27), 7459–7464. https://doi.org/10.1073/pnas.1520027113

Cohen, M. A., Konkle, T., Rhee, J. Y., Nakayama, K., & Alvarez, G. A. (2014). Processing multiple visual objects is limited by overlap in neural channels. *Proceedings of the National Academy of Sciences*, *111*(24), 8955–8960. https://doi.org/10.1073/pnas.1317860111

Cooreman, B., Wiegand, I., Petersen, A., Vangkilde, S., & Bundesen, C. (2015). Cue-it? We say: Block-it! *Journal of Vision*, *15*(12), 1335. https://doi.org/10.1167/15.12.1335

Cousineau, D. (2005). Confidence intervals in within-subject designs: A simpler solution to Loftus and Masson's method. *Tutorials in Quantitative Methods for Psychology*, *1*(1), 42–45. https://doi.org/10.20982/tqmp.01.1.p042

Cowan, N. (2001). The magical number 4 in short-term memory: A reconsideration of mental storage capacity. *The Behavioral and Brain Sciences*, *24*(1), 87–114. https://doi.org/10.1017/S0140525X01003922

Drew, T. W., McCollough, A. W., & Vogel, E. K. (2006). Event-related potential measures of visual working memory. *Clinical EEG and Neuroscience*, *37*(4), 286–291. https://doi.org/10.1177/155005940603700405

Drew, T., & Vogel, E. K. (2008). Neural measures of individual differences in selecting and tracking multiple moving objects. *Journal of Neuroscience*, *28*(16), 4183–4191. https://doi.org/10.1523/JNEUROSCI.0556-08.2008

Engle, R. W., Tuholski, S. W., Laughlin, J. E., & Conway, A. R. A. (1999). Working memory, short-term memory, and general fluid intelligence: A latent-variable approach. *Journal of Experimental Psychology: General*, *128*(3), 309–331. https://doi.org/10.1037/0096-3445.128.3.309

Ester, E. F., Sprague, T. C., & Serences, J. T. (2015). Parietal and frontal cortex encode stimulus-specific mnemonic representations during visual working memory. *Neuron*, *87*(4), 893–905. https://doi.org/10.1016/j.neuron.2015.07.013

Fahrenfort, J. J., Grubert, A., Olivers, C. N. L., & Eimer, M. (2016). Multivariate EEG analyses support high-resolution tracking of feature-based attentional selection. *BioRxiv*, 1–32, https://doi.org/10.1101/082818

Feldmann-Wüstefeld, T., Busch, N. A., & Schubö, A. (2019). Failed suppression of salient stimuli precedes behavioral errors. *Journal of Cognitive Neuroscience*, *32*(2), 367–377. https://doi.org/10.1162/jocn_a_01502

Feldmann-Wüstefeld, T., & Vogel, E. K. (2018). Neural evidence for the contribution of active suppression during working memory filtering. *Cerebral Cortex*, *29*(2), 529–543. https://doi.org/10.1093/cercovr/bhx336

Feldmann-Wüstefeld, T., Vogel, E. K., & Awh, E. (2018). Contralateral delay activity indexes working memory storage, not the current focus of spatial attention. *Journal of Cognitive Neuroscience*, *30*(8), 1185–1196. https://doi.org/10.1162/jocn_a_01271

Foster, J. J., Sutterer, D. W., Serences, J. T., Vogel, E. K., & Awh, E. (2016). The topography of alpha-band activity tracks the content of spatial working memory. *Journal of Neurophysiology*, *115*(1), 168–177. https://doi.org/10.1152/jn.00860.2015

Fukuda, K., Kang, M.-S., & Woodman, G. F. (2016). Distinct neural mechanisms for spatially lateralized and spatially global visual working memory representations. *Journal of Neurophysiology*, *116*(4), 1715–1727. https://doi.org/10.1152/jn.00991.2015

Fukuda, K., Mance, I., & Vogel, E. K. (2015). α power modulation and event-related slow wave provide dissociable correlates of visual working memory. *Journal of Neuroscience*, *35*(41), 14009–14016. https://doi.org/10.1523/JNEUROSCI.5003-14.2015

Gratton, G. (1998). The contralateral organization of visual memory: A theoretical concept and a research tool. *Psychophysiology*, *35*(6), 638–647. https://doi.org/10.1111/1469-8986.3560638

Herrero, J. L., Nikolaev, A. R., Raffone, A., & van Leeuwen, C. (2009). Selective attention in visual short-term memory consolidation. *NeuroReport*, *20*(7), 652–656. https://doi.org/10.1097/WNR.0b013e328329a431

Heuer, A., & Schubö, A. (2018). Separate and combined effects of action relevance and motivational value on visual working memory. *Journal of Vision*, *18*(5), 14. https://doi.org/10.1167/18.5.14

Holt, J. L., & Delvenne, J.-F. (2015). A bilateral advantage for maintaining objects in visual short term memory. *Acta Psychologica*, *154*, 54–61. https://doi.org/10.1016/j.actpsy.2014.11.007

Ikkai, A., McCollough, A. W., & Vogel, E. K. (2010). Contralateral delay activity provides a neural measure of the number of representations in visual working memory. *Journal of Neurophysiology*, *103*(4), 1963–1968. https://doi.org/10.1152/jn.00978.2009

Jolicœur, P., Brisson, B., & Robitaille, N. (2008). Dissociation of the N2pc and sustained posterior contralateral negativity in a choice response task. *Brain Research*, *1215*, 160–172. https://doi.org/10.1016/j.brainres.2008.03.059

Klaver, P., Smid, H. G. O. M., & Heinze, H.-J. (1999). Representations in human visual short-term memory: An event-related brain potential study. *Neuroscience Letters*, *268*(2), 65–68. https://doi.org/10.1016/S0304-3940(99)00380-8

Kleiner, M., Brainard, D., Pelli, D., Ingling, A., Murray, R., & Broussard, C. (2007). What's new in psychtoolbox-3. *Perception*, *36*(14), 1–16.

Klyszejko, Z., Rahmati, M., & Curtis, C. E. (2014). Attentional priority determines working memory precision. *Vision Research*, *105*, 70–76. https://doi.org/10.1016/j.visres.2014.09.002

Krumm, S., Ziegler, M., & Buehner, M. (2008). Reasoning and working memory as predictors of school grades. *Learning and Individual Differences*, *18*(2), 248–257. https://doi.org/10.1016/j.lindif.2007.08.002

Kuo, B.-C., Stokes, M. G., & Nobre, A. C. (2012). Attention modulates maintenance of representations in visual short-term memory. *Journal of Cognitive Neuroscience*, *24*(1), 51–60. https://doi.org/10.1162/jocn_a_00087

Lavie, N. (2005). Distracted and confused?: Selective attention under load. *Trends in Cognitive Sciences*, *9*(2), 75–82. https://doi.org/10.1016/j.tics.2004.12.004

Liesefeld, A. M., Liesefeld, H. R., & Zimmer, H. D. (2014). Intercommunication between prefrontal and posterior brain regions for protecting visual working memory from distractor interference. *Psychological Science*, *25*(2), 325–333. https://doi.org/10.1177/0956797613501170

Liu, S., Poh, J.-H., Koh, H. L., Ng, K. K., Loke, Y. M., Lim, J. K. W., … Zhou, J. (2018). Carrying the past to the future: Distinct brain networks underlie individual differences in human spatial working memory capacity. *NeuroImage*, *176*, 1–10. https://doi.org/10.1016/j.neuroimage.2018.04.014

Luck, S. J., & Vogel, E. K. (1997). The capacity of visual working memory for features and conjunctions. *Nature*, *390*(6657), 279–281. https://doi.org/10.1038/36846

Luck, S. J., & Vogel, E. K. (2013). Visual working memory capacity: From psychophysics and neurobiology to individual differences. *Trends in Cognitive Sciences*, *17*(8), 391–400. https://doi.org/10.1016/j.tics.2013.06.006

Luria, R., Balaban, H., Awh, E., & Vogel, E. K. (2016). The contralateral delay activity as a neural measure of visual working memory. *Neuroscience & Biobehavioral Reviews*, *62*, 100–108. https://doi.org/10.1016/j.neubiorev.2016.01.003

McEvoy, L. (1998). Dynamic cortical networks of verbal and spatial working memory: Effects of memory load and task practice. *Cerebral Cortex*, *8*(7), 563–574. https://doi.org/10.1093/cercor/8.7.563

Mecklinger, A., & Pfeifer, E. (1996). Event-related potentials reveal topographical and temporal distinct neuronal activation patterns for spatial and object working memory. *Cognitive Brain Research*, *4*(3), 211–224. https://doi.org/10.1016/S0926-6410(96)00034-1

Oberauer, K., Farrell, S., Jarrold, C., & Lewandowsky, S. (2016). What limits working memory capacity? *Psychological Bulletin*, *142*(7), 758–799. https://doi.org/10.1037/bul0000046

Phillips, W. A. (1974). On the distinction between sensory storage and short-term visual memory. *Perception & Psychophysics*, *16*(2), 283–290. https://doi.org/10.3758/BF03203943

Reinhart, R. M. G., & Woodman, G. F. (2014). High stakes trigger the use of multiple memories to enhance the control of attention. *Cerebral Cortex*, *24*(8), 2022–2035. https://doi.org/10.1093/cercor/bht057

Ruchkin, D. S., Johnson, R., Grafman, J., Canoune, H., & Ritter, W. (1992). Distinctions and similarities among working memory processes: An event-related potential study. *Cognitive Brain Research*, *1*(1), 53–66. https://doi.org/10.1016/0926-6410(92)90005-C

Ruchkin, D. S., Johnson, R., Grafman, J., Canoune, H., & Ritter, W. (1997). Multiple visuospatial working memory buffers: Evidence from spatiotemporal patterns of brain activity. *Neuropsychologia*, *35*(2), 195–209. https://doi.org/10.1016/S0028-3932(96)00068-1

Salahub, C. M., & Emrich, S. M. (2018). ERP evidence for temporal independence of set size and object updating in object substitution masking. *Attention, Perception, & Psychophysics*, *80*(2), 387–401. https://doi.org/10.3758/s13414-017-1459-6

Sander, M. C., Werkle-Bergner, M., & Lindenberger, U. (2011). Contralateral delay activity reveals life-span age differences in top-down modulation of working memory contents. *Cerebral Cortex*, *21*(12), 2809–2819. https://doi.org/10.1093/cercor/bhr076

Sauseng, P., Klimesch, W., Heise, K. F., Gruber, W. R., Holz, E., Karim, A. A., … Hummel, F. C. (2009). Brain oscillatory substrates of visual short-term memory capacity. *Current Biology*, *19*(21), 1846–1852. https://doi.org/10.1016/j.cub.2009.08.062

Schneider, D., Barth, A., Getzmann, S., & Wascher, E. (2017). On the neural mechanisms underlying the protective function of retroactive cuing against perceptual interference: Evidence by event-related potentials of the EEG. *Biological Psychology*, *124*, 47–56. https://doi.org/10.1016/j.biopsycho.2017.01.006

Simons, D. J., & Levin, D. T. (1997). Change blindness. *Trends in Cognitive Sciences*, *1*(7), 261–267. https://doi.org/10.1016/S1364-6613(97)01080-2

Thulasidas, M., Guan, C., & Jiankang, W. U. (2006). Robust classification of EEG signal for brain-computer interface. *IEEE Transactions on Neural Systems and Rehabilitation Engineering*, *14*(1), 24–29. https://doi.org/10.1109/TNSRE.2005.862695

Töllner, T., Conci, M., Rusch, T., & Müller, H. J. (2013). Selective manipulation of target identification demands in visual search: The role of stimulus contrast in CDA activations. *Journal of Vision*, *13*, 1–13. https://doi.org/10.1167/13.3.23.doi

Unsworth, N., Brewer, G. A., & Spillers, G. J. (2009). There's more to the working memory capacity—Fluid intelligence relationship than just secondary memory. *Psychonomic Bulletin & Review*, *16*(5), 931–937. https://doi.org/10.3758/PBR.16.5.931

Unsworth, N., Fukuda, K., Awh, E., & Vogel, E. K. (2014). Working memory and fluid intelligence: Capacity, attention control, and secondary memory retrieval. *Cognitive Psychology*, *71*, 1–26. https://doi.org/10.1016/j.cogpsych.2014.01.003

Unsworth, N., Fukuda, K., Awh, E., & Vogel, E. K. (2015). Working memory delay activity predicts individual differences in cognitive abilities. *Journal of Cognitive Neuroscience*, *27*(5), 853–865. https://doi.org/10.1162/jocn_a_00765

van Lamsweerde, A. E., & Beck, M. R. (2011). The change probability effect: Incidental learning, adaptability, and shared visual working memory resources. *Consciousness and Cognition*, *20*(4), 1676–1689. https://doi.org/10.1016/j.concog.2011.09.003

Vogel, E. K., & Machizawa, M. G. (2004). Neural activity predicts individual differences in visual working memory capacity. *Nature*, *428*(6984), 748–751. https://doi.org/10.1038/nature02447

Vogel, E. K., McCollough, A. W., & Machizawa, M. G. (2005). Neural measures reveal individual differences in controlling access to working memory. *Nature*, *438*(7067), 500–503. https://doi.org/10.1038/nature04171

Wiegand, I., Finke, K., Müller, H. J., & Töllner, T. (2013). Event-related potentials dissociate perceptual from response-related age effects in visual search. *Neurobiology of Aging*, *34*(3), 973–985. https://doi.org/10.1016/j.neurobiolaging.2012.08.002

Wiegand, I., Hennig-Fast, K., Kilian, B., Müller, H. J., Töllner, T., Möller, H.-J., … Finke, K. (2016). EEG correlates of visual short-term memory as neuro-cognitive endophenotypes of ADHD. *Neuropsychologia*, *85*, 91–99. https://doi.org/10.1016/j.neuropsychologia.2016.03.011

Wiegand, I., Lauritzen, M. J., Osler, M., Mortensen, E. L., Rostrup, E., Rask, L., … Petersen, A. (2018). EEG correlates of visual short-term memory in older age vary with adult lifespan cognitive development. *Neurobiology of Aging*, *62*, 210–220. https://doi.org/10.1016/j.neurobiolaging.2017.10.018

Wiegand, I., Töllner, T., Habekost, T., Dyrholm, M., Müller, H. J., & Finke, K. (2014). Distinct neural markers of TVA-based visual processing speed and short-term storage capacity parameters. *Cerebral Cortex*, *24*(8), 1967–1978. https://doi.org/10.1093/cercor/bht071

Xu, Z., Adam, K. C. S., Fang, X., & Vogel, E. K. (2018). The reliability and stability of visual working memory capacity. *Behavior Research Methods*, *50*(2), 576–588. https://doi.org/10.3758/s13428-017-0886-6

Zhang, W., & Luck, S. J. (2008). Discrete fixed-resolution representations in visual working memory. *Nature*, *453*(7192), 233–235. https://doi.org/10.1038/Nature06860

Zickerick, B., Thönes, S., Kobald, S. O., Wascher, E., Schneider, D., & Küper, K. (2020). Differential effects of interruptions and distractions on working memory processes in an ERP study. *Frontiers in Human Neuroscience*, *14*, 84. https://doi.org/10.3389/fnhum.2020.00084

How to cite this article: Feldmann-Wüstefeld T. Neural measures of working memory in a bilateral change detection task. *Psychophysiology*. 2021;58:e13683. https://doi.org/10.1111/psyp.13683